



HAL
open science

A three-source SVAT modeling of evaporation: Application to the seasonal dynamics of a grassed vineyard

Carlo Montes, Jean-Paul Lhomme, Jérôme Demarty, Laurent Prevo, Frédéric
Jacob

► **To cite this version:**

Carlo Montes, Jean-Paul Lhomme, Jérôme Demarty, Laurent Prevo, Frédéric Jacob. A three-source SVAT modeling of evaporation: Application to the seasonal dynamics of a grassed vineyard. *Agricultural and Forest Meteorology*, 2014, 191, pp.64–80. 10.1016/j.agrformet.2014.02.004 . hal-01863507

HAL Id: hal-01863507

<https://hal.science/hal-01863507v1>

Submitted on 5 Nov 2021

HAL is a multi-disciplinary open access archive for the deposit and dissemination of scientific research documents, whether they are published or not. The documents may come from teaching and research institutions in France or abroad, or from public or private research centers.

L'archive ouverte pluridisciplinaire **HAL**, est destinée au dépôt et à la diffusion de documents scientifiques de niveau recherche, publiés ou non, émanant des établissements d'enseignement et de recherche français ou étrangers, des laboratoires publics ou privés.

1
2
3
4
5
6
7
8
9
10
11
12
13
14
15

A three-source SVAT modeling of evaporation:
application to the seasonal dynamics of a grassed vineyard

Carlo Montes^{a*}, Jean-Paul Lhomme^a, Jérôme Demarty^b, Laurent Prévot^c and Frédéric Jacob^a

^a Institut de Recherche pour le Développement, UMR LISAH, 34060 Montpellier, France

^b Institut de Recherche pour le Développement, UMR HSM, 34095 Montpellier, France

^c Institut National de la Recherche Agronomique, UMR LISAH, 34060 Montpellier, France

* *Corresponding author address:*

Carlo Montes, UMR LISAH, 2 place Pierre Viala, 34060 Montpellier, France

E-mail address: ccmontesv@gmail.com

16 **Abstract.**

17

18 A parsimonious and versatile Soil-Vegetation-Atmosphere Transfer (SVAT) model is
19 proposed for three component vineyards, which includes vine foliage, grassed soil and bare
20 soil. A three-source energy balance approach describes the energy and mass transfer between
21 the soil-plant continuum and the lower atmosphere with an hourly time step. It is coupled with
22 a soil water balance module running with a daily time step. The model makes use of standard
23 meteorological data together with parameters describing foliage development, grass and soil
24 characteristics. The model is calibrated by means of the Multi-objective Calibration Iterative
25 Process (MCIP) algorithm and next validated for evaporation and soil moisture over a dataset
26 collected in a Southern France grassed vineyard. The validation exercise is twofold. It focused
27 first on the daily course of evaporation derived from the surface energy balance module only,
28 forced with weather variables, net radiation and soil moisture. The comparison against Eddy
29 Covariance measurements shows a good agreement ($R^2 = 0.96$ and $RMSE = 14.0 \text{ W m}^{-2}$).
30 Next, a simulation coupling the surface energy balance module with the soil water balance
31 module is validated over Eddy Covariance and soil moisture measurements. Simulations
32 throughout two contrasting growing seasons provide good estimates of daily evaporation (R^2
33 $= 0.90$ and $RMSE = 0.43 \text{ mm d}^{-1}$) and soil water content ($R^2 = 0.98$ and $RMSE = 6.95 \text{ mm}$).
34 Model inaccuracies arise mainly under conditions of strong surface runoff. Results also
35 suggest that the parameterizations relating the surface-atmosphere module with the soil
36 module (i.e. stomatal resistance) should be carefully examined under water stress conditions.
37 Finally, the model versatility is addressed through a set of static simulations. It appears that
38 the modeling approach allows assessing the seasonal water balance of vineyards differing by
39 their structure (varying grass fraction or distance between rows) and of similar cropping
40 systems.

41

42 **Key words:** latent heat flux; multi-source; sparse vegetation; soil water balance; seasonal
43 course

44

45

46

47

48 **List of symbols**

49

50 A_i : available energy for each component vs and bs ($W\ m^{-2}$)

51 A_f : available energy for the main foliage ($W\ m^{-2}$)

52 c : radiation extinction coefficient by canopy

53 c_p : specific heat of air at constant pressure ($J\ kg^{-1}\ K^{-1}$)

54 CR_3 : capillary rise into reservoir (3) (mm)

55 d : displacement height (m)

56 D_1 : drainage from reservoir (1) to (3) (mm)

57 D_2 : drainage from reservoir (2) to (3) (mm)

58 D_3 : deep percolation from reservoir (3) (mm)

59 D_a : vapor pressure deficit at reference height (Pa)

60 D_m : vapor pressure deficit at mean canopy source height (Pa)

61 e_a : vapor pressure at reference height (Pa)

62 $e^*(T_i)$: saturated vapor pressure at temperature T_i ($i = f, vs, bs$) (Pa)

63 F_{bs} : fraction of bare soil ($= 1 - F_{vs}$)

64 F_{vs} : fraction of vegetated soil

65 $F_1 = F_{bs}$

66 $F_2 = F_{vs}$

67 G_{vs} : soil heat flux of vegetated soil ($W\ m^{-2}$)

68 G_{bs} : soil heat flux of bare soil ($W\ m^{-2}$)

69 I_{vs} : infiltration term for vegetated soil (mm)

70 I_{bs} : infiltration term for bare soil (mm)

71 $K(z_h)$: turbulent diffusivity at canopy height ($m^2\ s^{-1}$)

72 L : Monin-Obukhov length (m)

73 LAI_f : leaf area index of main foliage ($m^2\ m^{-2}$)

74 $CLAI_{vs}$: clumped leaf area index of vegetated soil ($m^2\ m^{-2}$)

75 n : parameter with value of 1 for amphistomatous and 2 for hypostomatous foliage

76 r_a : aerodynamic resistance between the mean source height (z_m) and the reference height (z_r , s
77 m^{-1})

78 $r_{a,i}$: aerodynamic resistance between the evaporative source ($i = vs, bs$) and mean source
79 height (z_m , $s\ m^{-1}$)

80 $r_{a,f,h}$: bulk boundary-layer resistance of the foliage for sensible heat ($s\ m^{-1}$)

- 81 $r_{s,i}$: surface resistance (stomatal or soil surface) for each source ($i = f, vs, bs$) ($s\ m^{-1}$)
- 82 R_n : net radiation of the whole canopy ($W\ m^{-2}$)
- 83 u_a : wind speed at reference height ($m\ s^{-1}$)
- 84 z_h : height of the main foliage (m)
- 85 z_m : mean source height (m)
- 86 z_r : reference height (m)
- 87 z_0 : roughness length for momentum of main foliage (m)
- 88 z_0^i : roughness length for momentum of vegetated ($i = vs$) or bare soil ($i = bs$) (m)
- 89 z_1 : depth of soil reservoir (1) (m)
- 90 z_2 : depth of soil reservoir (2) (m)
- 91 z_R : vines rooting depth (m)
- 92 z_G : water table depth (m)
- 93 γ : psychrometric constant ($Pa\ K^{-1}$)
- 94 λ : latent heat of vaporization ($J\ kg^{-1}$)
- 95 Δ : slope of the saturated vapor pressure curve at air temperature ($Pa\ K^{-1}$)
- 96 ρ : air density ($kg\ m^{-3}$)
- 97 ϕ_s : solar zenith angle (radians)
- 98
- 99

1. Introduction

Progress in theoretical and applied research aiming at accurately assessing crop water consumption in both rain-fed and irrigated conditions is an essential issue for agricultural water management. Since evaporation measurements are scarce, operational formulations to estimate water consumption at field scale are necessary (Trambouze et al., 1998; Spano et al., 2009). For viticulture regions in Mediterranean and semi-arid environments, actual evaporation represents a major component of surface water balance, reaching up to 70% of the yearly precipitation (Moussa et al., 2007). Knowledge of actual evaporation is also of interest in viticulture, in order to assess and handle the influence of soil water deficit on grapevine yields and berry composition (Vaudour, 2003; Pellegrino et al., 2005). Nevertheless, the physical representation of the soil-plant-atmosphere system in grapevines is a complex issue, because the sparse structure of vineyards imposes to consider both the foliage and the understory, which requires multi-source modeling.

The most frequently used multi-source evaporation model is the one first developed by Shuttleworth and Wallace (1985) (S-W model) and extended by Choudhury and Monteith (1988) and Shuttleworth and Gurney (1990). This model corresponds to an extension of the big-leaf model of Penman-Monteith (Monteith, 1965) into two interacting evaporative layers: the main foliage and the underlying substrate. Subsequently, the S-W model was upgraded by Brenner and Incoll (1997) (“clumped” model) to account for three sources of evaporation after dividing the understory into a bare soil fraction and a soil fraction below the main foliage, and also by Verhoef and Allen (2000) to account for four sources of evaporation. The two- and three-source formalisms were revisited by Lhomme et al. (2012) to propose more concise and accurate formulations and to account for foliage morphological characteristics (amphistomatous versus hypostomatous leaves). All these models are based on the diffusion theory (*K*-theory) for energy and mass transfer within the lower atmosphere. More complex models based on higher order Lagrangian and Eulerian dispersion processes can be found in the literature: they allow a better representation of vegetation-atmosphere turbulent transfers (Raupach, 1989; Yi, 2008), but their complexity and data requirement make them difficult to use in a practical modeling framework. It has been shown, further, that the diffusion theory is appropriate to represent the microclimate at canopy scale in comparison with Lagrangian representations (van den Hurk and McNaughton, 1995; Wu et al., 2001).

One of the first models to estimate vineyard evaporation is the one proposed by Riou et al. (1989, 1994). It is not a multi-source model: vineyard evaporation under unstressed

134 conditions is expressed as a simple function of potential evaporation and solar radiation
135 intercepted by the canopy. This model was extended later by Trambouze and Voltz (2001),
136 who derived a bilinear relationship relating the ratio between vineyard actual and maximum
137 transpiration to the average soil water storage. Subsequently, several authors have applied the
138 multi-source resistance-based formulations to assess vineyard evaporation. First, we have to
139 mention the work by Rana and Katerji (2008), where a simple single-source model (Penman-
140 Monteith) was applied to vineyards trained on overhead system. In an earlier work by Sene
141 (1994), the more complex S-W model was applied with the purpose of interpreting energy
142 balance measurements over a sparse vineyard in southern Spain. More recently, an
143 appropriate representation of total latent heat flux from a drip-irrigated vineyard in central
144 Chile was obtained by Ortega-Farias et al. (2007) by applying the same S-W model. In
145 addition, Poblete-Echeverria and Ortega-Farias (2009) adapted the so-called “clumped”
146 model to drip irrigation over the same region of Chile by dividing the substrate (bare soil) into
147 a dry and a wet (irrigated) portion. Zhang et al. (2008) compared these two models (S-W and
148 clumped) against Bowen ratio estimates in a semi-arid vineyard of China: they concluded that
149 the clumped model was more suitable to estimate total vineyard evaporation than the S-W
150 model. On the same basis, Zhang et al. (2009) elaborated a multi-source S-W type model to
151 simulate the evaporation from a vineyard under partial root-zone irrigation, taking into
152 consideration different patches of soil.

153 All these vineyard evaporation models, however, do not take into account the common
154 practice of maintaining a permanent or semi-permanent grass cover. This consists in a seeded
155 or natural grass cover in between vine rows, maintaining bare soil on the rows. This practice
156 is increasingly used because it has several positive impacts, such as the reduction in rainfall
157 erosive potential and surface runoff, the reduction in nutrient lixiviation, the decrease in vine
158 vigor and grape production (which improves grapes quality) and the improvements in soil
159 structure and trafficability after rainfall events (Pradel and Pieri, 2000; Morlat and Jacquet,
160 2003; Celette et al., 2005; Celette et al., 2008; Gaudin et al., 2010). As compared with the
161 traditional bare soil grapevine cultivation, the grass cover affects energy and water balance
162 since surface albedo, net radiation partitioning, water consumption and infiltration are
163 modified (Rodriguez-Iturbe, 2000; Zhang and Schilling, 2006; Centinari et al., 2012). For
164 instance, in a recent work by Holland et al. (2013) on grassed vineyard, significant differences
165 were found between grassed and bare soil energy partitioning. Therefore, this grass cover
166 component should be considered into a modelling formulation.

167 In addition, most of the vineyard evaporation models mentioned above only consider

168 above-ground processes (i.e. vegetation and soil surface), which interact with soil water
169 through the parameterization of a stomatal or substrate resistance to evaporation, in the best
170 case. Thus, they do not allow the temporal dynamics of vineyard evaporation to be adequately
171 simulated throughout the season. However, models have been developed to simulate soil
172 water balance of vineyards. Sene (1996) was the first to combine a simple soil moisture model
173 with a two-component (S-W) representation of vineyard evaporation in order to estimate the
174 long-term water balance of a sparse vine crop growing under semi-arid conditions. Lebon et
175 al. (2003) also performed simulations of the seasonal dynamics of soil water balance in
176 vineyards by using a single reservoir soil model along with the Riou et al. (1989, 1994)
177 approach for grapevine transpiration coupled with a stress function involving soil water
178 availability (Trambouze and Voltz, 2001). Celette et al. (2010) extended the model of Lebon
179 et al. (2003) to simulate the water balance of an intercropped vineyard considering an
180 additional and separate soil compartment under the cover crop. Galleguillos et al. (2011) also
181 used the model of Riou et al. (1989, 1994), but coupled with the HYDRUS-1D simulation
182 model of soil water transfers. Although realistic results have been obtained with this type of
183 soil water balance model, the evaporation process remains poorly represented and a more
184 realistic approach based upon micrometeorological resistance-type models coupled with soil
185 water models appears to be necessary.

186 With regards to the elements discussed above, the main objective of the present work
187 is to develop a Soil-Vegetation-Atmosphere Transfer (SVAT) model which simulates the
188 vineyard evaporation dynamics at seasonal scale and accounts for the grass cover as a
189 viticultural practice. It combines a comprehensive micrometeorological three-source model of
190 evaporation with a three reservoir soil water balance model. The formulation is versatile
191 enough to allow the assessment of evaporation rate from different mixed cropping systems, in
192 so far as species-specific biophysical parameters and physical soil properties descriptors are
193 adjusted to the prevailing conditions. The formulation is also kept as parsimonious as possible
194 to foresee its application at the regional extent while accounting for the inter-field variability.
195 The plan is as follows. In Section 2, the SVAT model is fully described, separating the
196 evaporation model from the soil water balance model. Section 3 details the study area, the
197 experimental data, the model implementation and the strategy for calibration. Section 4 shows
198 a comparison of model simulations against ground truth data to validate the model and some
199 simulations are presented to show the versatility of the model through its aptitude to represent
200 different viticultural practices (proportion of grassed soil and distance between rows). Finally,
201 model results and limitations are discussed in Section 5.

202

203 **2. Model development**

204

205 **2.1 Representing the vine-grass-soil system**

206

207 The soil-plant-atmosphere continuum is represented as a three-source system that
208 includes the vine canopy (main foliage) and a composite substrate made of a grass cover and
209 bare soil. This rain fed Cabernet Sauvignon vineyard is conducted in rows. Vine leaf area
210 index (LAI_f) varies throughout the growing season from 0 to a maximum value and next falls
211 back to 0 during senescence. The grass cover is present only on one inter-row out of two. It is
212 characterized by the concept of clumped LAI ($CLAI_{vs}$), defined as grass leaf area index per
213 unit area of grass cover: $CLAI_{vs} = LAI_{vs}/F_{vs}$, F_{vs} being the proportion of vegetated soil. Grass
214 exhibits a seasonal dynamics: its growth is initiated by autumn precipitations and it dries off
215 in early summer as a result of large water stress. The bare soil fraction (F_{bs}) covers the rest of
216 the inter-row and the soil below the vines. The vine-grass-soil system corresponds to a three-
217 source system between autumn and early summer and to a two-source system in summer,
218 when the substrate is made of bare soil and dry grass only ($F_{bs} = 1$).

219 The three components should be considered separately because they have different
220 physical and geometrical features which affect energy and mass transfers. Nevertheless, the
221 vine patches are not large enough to adopt a patch representation of the whole system and
222 consequently a layer representation is preferred (Boulet et al., 1999; Lhomme and Chehbouni,
223 1999; Anderson et al., 2005). Given the composite nature of the substrate, the modeling
224 combines a layer approach for the vine-substrate system with a patch approach for the
225 substrate (grass cover + bare soil), as represented in Fig. 1 and explained in Lhomme et al.
226 (2012, section 3.1). Indeed, while substrate and vine are interrelated in the vertical transfer of
227 heat and water vapor with a sole aerodynamic resistance above the whole canopy, grass cover
228 and substrate are assumed to act separately vis-a-vis the canopy source height.

229 Soil moisture dynamics is represented by a bucket type model made of three reservoirs
230 in relation with the three components of the evaporation model: a deep reservoir
231 corresponding to the vine rooting system (~2 m) and two shallow reservoirs corresponding to
232 the two substrate components. The main input of the system corresponds to the infiltration of
233 water from precipitation. Drainage processes control the water transfers between reservoirs.
234 Evaporation is the main output and deep percolation acts as a secondary output. Capillary rise
235 from the saturated zone below the deep reservoir is also considered, but horizontal water

236 transfers (runoff) are ignored.

237 The SVAT model consists of coupling the surface energy balance for plant-
238 atmosphere system and the soil water balance for the subsurface system. The evaporation
239 model runs with a short time step (one hour or less) and is forced with meteorological data
240 (air temperature and humidity, wind speed, solar radiation) and vegetation data (vine height
241 and leaf area, fraction of grass cover). The soil water balance runs on a daily time step and is
242 forced with daily precipitation. The water content of each subsurface reservoir is an input to
243 the corresponding evaporation components and conversely the evaporation components are
244 inputs for the soil water balance module.

245

246 2.2 Evaporation model

247

248 We detail hereafter the surface energy balance and soil water balance modules
249 forming the SVAT model and their corresponding parameterizations. For the numerous
250 formulations considered in this section, the values of the corresponding parameters are given
251 in Table 1.

252

253 2.2.1 Formulation of evaporation

254

255 The total flux of latent heat (λE_t) is the sum of the contributions from three sources:
256 main foliage (λE_f), vegetated soil (λE_{vs}) with relative area F_{vs} and bare soil (λE_{bs}) with relative
257 area $F_{bs} = 1 - F_{vs}$. They are aggregated following a coupled (or layer) approach (Fig. 1):

258

$$259 \lambda E_t = \lambda E_f + \lambda E_{vs} + \lambda E_{bs}. \quad (1)$$

260

261 The three evaporation components reach the mean canopy source height (z_m), assumed to be
262 located at the apparent sink for momentum (zero plane displacement height $d +$ roughness
263 length z_0), where they mix together forming the total evaporation at reference height (z_r) as it
264 can be measured with Bowen ratio or Eddy Covariance system. The resistances network
265 represents the controlling effects of soil surface, stomatal behavior and surrounding air, which
266 are considered to be “in series” for each individual source. Vegetated (vs) and bare soil (bs)
267 air resistances extend from the surface level ($z_{0,i}$, $i = vs$ or bs) to the mean canopy source
268 height (z_m). Evaporation components are calculated from Penman-Monteith type equations

269 involving the corresponding available energy (A_f , A_{vs} or A_{bs}) and the vapor pressure deficit D_m
 270 at mean canopy source height z_m . However, following Lhomme et al. (2012), the stomatal
 271 characteristics of the main foliage (amphistomatous or hypostomatous) are taken into account
 272 in the evaporation formulation

273

$$274 \quad \lambda E_f = \frac{\Delta A_f + \rho c_p D_m / r_{a,f,h}}{\Delta + \gamma (n + r_{s,f} / r_{a,f,h})}, \quad (2)$$

275

276 where the parameter n takes the value $n = 1$ for amphistomatous and $n = 2$ for hypostomatous
 277 leaves. Since grapevine foliage is hypostomatous, we took $n = 2$. Δ is the slope of the
 278 saturated vapor pressure curve at air temperature, ρ the air density, c_p the specific heat of air
 279 at constant pressure, γ the psychrometric constant, $r_{a,f,h}$ the foliage bulk boundary-layer
 280 resistance for sensible heat and $r_{s,f}$ the bulk surface resistance of the foliage. For the two
 281 substrate components (vegetated soil and bare soil) we have

282

$$283 \quad \lambda E_i = \frac{\Delta A_i + \rho c_p D_m / r_{a,i}}{\Delta + \gamma (1 + r_{s,i} / r_{a,i})}, \quad \text{with } i = vs \text{ or } bs \quad (3)$$

284

285 $r_{a,i}$ is the aerodynamic resistance between the evaporative source ($i = vs, bs$) and z_m , and $r_{s,i}$ is
 286 the surface resistance (stomatal or soil surface) for each source ($i = vs, bs$).

287 The total evaporation per unit area from the whole canopy is obtained using the
 288 formulation developed by Lhomme et al. (2012, Eq. (33)) for a three-source evaporative
 289 surface:

290

$$291 \quad \lambda E_t = \left(\frac{\Delta + \gamma}{\gamma} \right) \left(P_f + P_{vs} + P_{bs} \right) \lambda E_p + \frac{\Delta}{\gamma} \left(P_f r_{a,f,h} A_f + P_{vs} r_{a,vs} A_{vs} + P_{bs} r_{a,bs} A_{bs} \right) / r_a, \quad (4)$$

292

293 where λE_p represents the potential evaporation expressed as

294

$$295 \quad \lambda E_p = \frac{\Delta A + \rho c_p D_a / r_a}{\Delta + \gamma}, \quad (5)$$

296

297 where A is the total available energy and r_a is the aerodynamic resistance between the source
 298 height z_m and the reference height z_r . The P_i coefficients of Eq. (4) are combinations of
 299 surface and aerodynamic resistances, detailed in Appendix A. Each evaporation component is
 300 obtained from Eqs. (2) and (3) by expressing the in-canopy vapor pressure deficit D_m as a
 301 function of the saturation deficit at reference height D_a (Shuttleworth and Wallace, 1985):

$$302 \quad D_m = D_a + \left[\Delta A - \lambda E_t (\gamma + \Delta) \right] r_a / (\rho c_p). \quad (6)$$

304

305 2.2.2 Partition of available energy

306

307 Total available energy (A) for turbulent fluxes is defined as the difference between the
 308 total net radiation (R_n) and the soil heat flux (G) counted positively when gained by the
 309 surface: $A = R_n - G$. Beer's law is used to obtain the partitioning of net radiation including the
 310 effects of solar zenith angle (ϕ_s) on net radiation extinction (Anderson et al., 1997; Kustas et
 311 al., 1998). Considering the canopy as a semi-transparent layer to incident radiation, the net
 312 radiation reaching the substrate level $R_n(0)$ is obtained by

$$313 \quad R_n(0) = R_n \exp\left(-cLAI_f / \sqrt{2 \cos(\phi_s)}\right), \quad (7)$$

315

316 where c is the extinction coefficient of radiation of the main foliage, which depends upon
 317 leaves angular distribution (Choudhury, 1989), and LAI_f its leaf area index. For the main
 318 vegetation canopy, the available energy (A_f) is computed as the difference between the total
 319 net radiation above the canopy and that reaching the substrate level:

320

$$321 \quad A_f = R_n - R_n(0) = R_n \left[1 - \exp\left(-cLAI_f / \sqrt{2 \cos(\phi_s)}\right) \right]. \quad (8)$$

322

323 Soil heat flux for vegetated and bare soil (G_{vs} and G_{bs} , respectively) is obtained as a
 324 fraction of the net radiation reaching the substrate level (Norman et al., 1995; Boulet et al.,
 325 2000). Per unit area of substrate we have $G_{vs} = \beta_{vs} R_n(0)$ and $G_{bs} = \beta_{bs} R_n(0)$, β_{vs} and β_{bs}
 326 representing the proportions of residual net radiation conducted into the soil. Available energy
 327 for vegetated (A_{vs}) and bare soil (A_{bs}) is respectively obtained as

328

329 $A_{vs} = F_{vs} [R_n(0) - G_{vs}] = F_{vs} (1 - \beta_{vs}) \exp(-cLAI_f / \sqrt{2 \cos(\phi_s)}) R_n,$ (9)

330

331 $A_{bs} = F_{bs} [R_n(0) - G_{bs}] = F_{bs} (1 - \beta_{bs}) \exp(-cLAI_f / \sqrt{2 \cos(\phi_s)}) R_n,$ (10)

332

333 and consequently

334

335 $A = R_n - G = R_n [1 - \exp(-cLAI_f / \sqrt{2 \cos(\phi_s)}) (F_{vs} \beta_{vs} + F_{bs} \beta_{bs})].$ (11)

336

337 2.2.3 Net radiation estimation

338

339 The evaporation formulations detailed in Section 2.2.1 consider that the net radiation
340 of the whole surface constitutes an input to the model. It is expressed as

341

342 $R_n = (1 - a)R_g + \varepsilon(R_{atm} - \sigma T_R^4),$ (12)

343

344 where a is the effective surface albedo, R_g the incoming shortwave or solar radiation, R_{atm} the
345 downward longwave or atmospheric radiation, ε the surface longwave emissivity, σ the
346 Stefan-Boltzmann constant and T_R the composite radiometric temperature of the surface (main
347 foliage and substrate).

348 Net radiation, however, is not commonly and routinely measured. Given that the
349 purpose of this work is to develop an operational and dynamic version of the model running
350 with meteorological inputs, R_n should be determined beforehand. If R_g is generally measured
351 and R_{atm} measured or easily calculable from air temperature and humidity, T_R is an unknown
352 variable which cannot be considered as an input to the model. It can be expressed as a
353 function of the component temperatures in the following way based on the Stefan-Boltzmann
354 law (Norman et al., 1995):

355

356 $T_R = [f_0 T_f^4 + (1 - f_0) T_s^4]^{1/4},$ (13)

357

358 where T_f is the temperature of the main foliage and T_s is the composite substrate temperature
359 expressed as a weighted mean of the component temperatures

360

361 $T_s = F_{vs}T_{vs} + F_{bs}T_{bs}$. (14)

362

363 In Eq. (13) f_0 represents the fractional vegetation cover obtained by

364

365 $f_0 = 1 - \exp(-cLAI_f)$, (15)

366

367 with c the same coefficient as in Eq. (7) and LAI_f the leaf area index of the main foliage.
 368 Given that surface temperature T_R is required to solve Eq. (12), an iterative procedure is
 369 implemented to obtain the corresponding surface temperatures (T_f , T_{vs} , T_{bs}). An initial loop
 370 sets $T_i = T_a$ ($i = f, vs, bs$) to solve Eqs. (12) to (15) and to calculate the distribution of available
 371 energy from Eqs. (7) to (11). Eqs. (4) to (6) are then used to calculate λE_t and D_m , which
 372 allows calculating a new set of component surface temperatures T_i , which are reintroduced
 373 into Eq. (13) until the convergence is achieved. The details of surface temperatures
 374 calculation are presented in Appendix B.

375 The effective albedo for shortwave radiation (a in Eq. (12)) is obtained using the
 376 following expression (Taconet et al., 1986; Lhomme and Monteny, 2000):

377

378 $a = f_0 a_f + \frac{a_s (1 - f_0)^2}{(1 - f_0 a_f a_s)}$, (16)

379

380 where a_f and a_s are the albedos of the main foliage and of the substrate, respectively. Substrate
 381 albedo a_s is calculated as a simple weighted component albedo: $a_s = F_{bs} a_{bs} + F_{vs} a_{vs}$, with a_{vs}
 382 and a_{bs} the albedo of the vegetated and bare soil, respectively.

383

384 2.2.4 Parameterizations of surface and aerodynamic resistances

385

386 *Surface resistances*

387

388 The main foliage surface resistance to vapor transfer is parameterized using the widely
 389 used Jarvis-type analytical formulation (Jarvis, 1976). This formulation links the stomatal
 390 conductance (inverse of resistance) to environmental factors controlling the relative stomatal
 391 closure: photosynthetically active radiation (PAR_f), vapor pressure deficit (D_a) and soil water

392 content (θ_f). It is expressed as

393

$$394 \quad g_{s,f} = 1/r_{s,f} = (g_{x,f} LAI_f) f_1(PAR_f) f_2(D_a) f_3(\theta_f), \quad (17)$$

395

396 where $g_{x,f}$ is the maximum leaf stomatal conductance, observed when environmental factors
397 are not limiting. Each function represents a stress function with values between 0 and 1. They
398 are defined as

399

$$400 \quad f_1(PAR_f) = 1 - \exp(-PAR_f/K_1^f), \quad (18)$$

401

$$402 \quad f_2(D_a) = 1 - K_2^f D_a, \quad (19)$$

403

404 where PAR_f is the photosynthetically active radiation reaching the main foliage (calculated as
405 a fraction of solar radiation); K_1^f and K_2^f are two empirical parameters. The stress function
406 for soil water content is parameterized considering a negative exponential relationship
407 between stomatal conductance and soil water deficit (Stewart, 1988). This relationship is
408 defined as

409

$$410 \quad f_3(\theta_f) = 1 - \exp\left[-K_3^f(\theta_f - \theta_{f,wp})\right], \quad (20)$$

411

412 with θ_f the volumetric soil moisture averaged over the depth of the rooting system, $\theta_{f,wp}$ its
413 moisture at wilting point and K_3^f a fitting parameter.

414 Grass cover conductance is calculated using the same formulation as above (subscript
415 f is replaced by subscript vs), but with specific parameters and coefficients. However, since
416 grass occupies only a portion of the representative area (F_{vs}), the stomatal conductance should
417 be multiplied by this relative area (Lhomme et al., 2012). Local observations indicate that the
418 inter-row grass cover extends its vegetative cycle until early summer and then completely
419 dries out, which means that stomatal conductance becomes equal to zero and only soil
420 evaporation should be considered, then F_{vs} is set to zero.

421 Direct evaporation from topsoil layers is regulated by complex processes that can be
422 summarized in a soil surface resistance $r_{s,bs}$. A wide list of formulations for this physical

423 control on evaporation can be found in the literature, most of them relating $r_{s,bs}$ to local
 424 observations of soil water content (e.g. Mahfouf and Noilhan 1991). This resistance was
 425 parameterized using the formulation proposed by Sellers et al. (1992), divided by bare soil
 426 relative area:

$$428 \quad r_{s,bs} = \exp(A_1 - B_1 \theta_{bs} / \theta_{s,bs}) / F_{bs}, \quad (21)$$

429
 430 with θ_{bs} and $\theta_{s,bs}$ the actual and saturated water content of the upper soil layer; A_1 and B_1 are
 431 fitting parameters.

432 433 *Aerodynamic resistances*

434
 435 The aerodynamic resistance between canopy source height (z_m) and reference height
 436 (z_r), assumed to be the same for heat and water transfer, is calculated using the formulation
 437 proposed by Brutsaert (1982), which takes into account the stability correction functions for
 438 momentum and heat under non-neutral conditions. The boundary layer resistance of the main
 439 foliage is estimated using the formulation proposed by Choudhury and Monteith (1988). The
 440 aerodynamic resistances between the substrate and the mean canopy source ($r_{a,vs}$ and $r_{a,bs}$) are
 441 defined by the integral of the inverse of the eddy diffusivity (Choudhury and Monteith, 1988;
 442 Shuttleworth and Gurney, 1990). All these aerodynamic resistances are detailed in Appendix
 443 C. For substrate components, the aerodynamic resistances should be weighted by their relative
 444 area, as highlighted by Lhomme et al. (2012). If $r_{a,i}^1$ ($i = vs, bs$) is the aerodynamic resistance
 445 per unit area of component substrate with relative area F_i , the aerodynamic resistance per unit
 446 area of land surface should be written as $r_{a,i} = r_{a,i}^1 / F_i$.

447 448 **2.3 Water balance model**

449 450 2.3.1 Soil water equations

451
 452 To simulate the water budget seasonal dynamics, the evaporation model described in
 453 section 2.2, which is run with an hourly time step, is coupled with a soil water balance module
 454 run with a daily time step. The daily time step was selected for feasibility reasons, since daily

455 values of rainfall are usually more available than hourly values. The soil layer beneath the
 456 vegetation is divided into three finite reservoirs (Fig. 1): a reservoir (1), located just below the
 457 bare soil component with relative area $F_1 = F_{bs}$ and depth z_1 ; reservoir (2), located just below
 458 the vegetated soil with relative area $F_2 = F_{vs}$ and depth z_2 ; and reservoir (3), located below
 459 reservoirs (1) and (2), which extends to a depth z_R taken as equal to the vines rooting depth.
 460 Available water content of each soil compartment is considered as uniformly distributed over
 461 the corresponding soil profile. Bare soil and vegetated soil evaporation occur respectively
 462 from reservoir 1 and 2. Main foliage is supposed to extract water both from reservoirs 2 and 3,
 463 because the rooting system of vines is expected to extend within that of grass. A saturated
 464 zone with depth z_G is also considered, which potentially can rise to reach the bottom of
 465 reservoir (3).

466 Horizontal water transfers, as well as surface runoff, are considered out of the scope of
 467 this one-dimensional modeling approach and are ignored. In any case, the runoff component
 468 can be added (or subtracted) to the infiltration term of the water balance. Thus, the main water
 469 input to the system corresponds to the infiltration of water from precipitation to reservoirs (1)
 470 and (2). Root water uptake by the vineyard and grass, and bare soil evaporation correspond to
 471 the main water outputs. Transfers from reservoirs (1) and (2) to (3), and from (3) to the
 472 saturated zone are carried out through percolation process. Capillary rise from the saturated
 473 zone to reservoir (3) can also act as a secondary input of water. Capillary rise from reservoir
 474 (3) to surface reservoirs (1) and (2) is assumed to be negligible.

475 Soil water capacity TSW_i (total soil water) for each reservoir is defined as the
 476 difference between the amount of water stored at field capacity and a minimum amount,
 477 specified below. It is calculated as a function of its depth and relative area F_i

478
 479
$$TSW_i = 1000 F_i z_i (\theta_{fc,i} - \theta_{n,i}) (1 - p_i), \quad i = 1 \text{ or } 2 \quad (22)$$

480
 481
$$TSW_3 = 1000 [F_2 (z_R - z_2) + F_1 (z_R - z_1)] (\theta_{fc,3} - \theta_{n,3}) (1 - p_3), \quad (23)$$

482
 483 TSW_i is expressed in mm and the reservoir depth z_i in m, θ_i is the volumetric humidity in
 484 $\text{m}^3 \text{m}^{-3}$ (subscript fc indicates field capacity and n a minimum value), p_i is the fractional stone
 485 content, and the value 1000 is a conversion factor. Similarly, available soil water (ASW_i) of
 486 each reservoir is defined as the difference between its actual water content (θ_i) and its content
 487 at a minimum value ($\theta_{n,i}$). It is expressed by the same equations as (22) and (23), where $\theta_{fc,i}$ is

488 replaced by θ_i . For reservoir (2) the minimum humidity ($\theta_{n,2}$) is taken to be equal to that at
 489 wilting point ($\theta_{vs,wp}$). For reservoirs (1) and (3), the minimum humidity $\theta_{n,i}$ is set to minimum
 490 values below wilting point, as observed by Trambouze and Voltz (2001) on the same plot
 491 (Table 2).

492 The root system of the main vegetation is supposed to extract water from
 493 compartments (1) and (2). The grass cover extracts water only from reservoir (2) and bare soil
 494 evaporation comes from reservoir (1) which is only a few centimeters deep. The amount of
 495 water (ASW_i) stored into each of the three compartments is calculated following a dynamic
 496 process with a daily budget (subscript j):

497

$$498 \quad ASW_{1,j} = ASW_{1,(j-1)} + I_{1,j} - E_{1,bs,j} - D_{1,j}, \quad (24)$$

499

$$500 \quad ASW_{2,j} = ASW_{2,(j-1)} + I_{2,j} - E_{2,vs,j} - E_{2,f,j} - D_{2,j}, \quad (25)$$

501

$$502 \quad ASW_{3,j} = ASW_{3,(j-1)} + I_{3,j} + CR_{3,j} - E_{3,f,j} - D_{3,j}. \quad (26)$$

503

504 The infiltration terms are denoted by I , the percolation terms by D and the evaporation
 505 terms by E . All the terms are expressed in mm d^{-1} . The water inputs for vegetated and bare
 506 soil reservoirs are daily rainfall (P_j) weighted by their relative area (F_i), so $I_{i,j} = F_i P_j$ ($i = 1$ and
 507 2). The infiltration into the third reservoir ($I_{3,j}$) is expressed as the sum of the drainage
 508 components of the upper reservoirs as $I_{3,j} = D_{1,j} + D_{2,j}$. For each reservoir, percolation is
 509 calculated as the amount of water in excess with respect to the total available water: it is the
 510 positive difference between the sum of inputs and the water holding capacity of the reservoir
 511 defined as the difference between TSW_i and ASW_i . For the surface compartments ($i= 1$ and 2)
 512 we have

513

$$514 \quad D_{i,j} = I_{i,j} - (TSW_i - ASW_{i,j}) \quad \text{if} \quad I_{i,j} > (TSW_i - ASW_{i,j}), \quad (27)$$

515

$$516 \quad D_{i,j} = 0 \quad \text{if} \quad I_{i,j} \leq (TSW_i - ASW_{i,j}), \quad (28)$$

517

518 and for compartment (3)

519

520 $D_{3,j} = (D_{1,j} + D_{2,j}) - (TSW_3 - ASW_{3,j})$ if $(D_{1,j} + D_{2,j}) > (TSW_3 - ASW_{3,j})$, (29)

521

522 $D_{3,j} = 0$ if $(D_{1,j} + D_{2,j}) \leq (TSW_3 - ASW_{3,j})$. (30)

523

524 Given that the evaporation module is run with a time step shorter than one day (e.g. 1
 525 hour), the evaporation terms are calculated as the 24 hours summation. The partitioning of
 526 main foliage evaporation between the two compartments (2) and (3) is obtained through a
 527 simple weighting by the relative soil water content of these two compartments.
 528 Putting $ASW_f = ASW_2 + ASW_3$, we have respectively

529

530 $E_{2,f,j} = \frac{ASW_2}{ASW_f} \sum_{h=1}^{24} E_{f,j,h}$ and $E_{3,f,j} = \frac{ASW_3}{ASW_f} \sum_{h=1}^{24} E_{f,j,h}$, (31)

531

532 where $E_{f,j,h}$ is the evaporation from the main foliage in mm h^{-1} . In Eq. (31), evaporation
 533 components E_f , E_{vs} and E_{bs} are obtained by Eqs. (2) and (3).

534 Since the main foliage extracts water from compartments (2) and (3), the soil water
 535 content (θ_f) involved in its stress function (Eq. (20)) is calculated as the mean of the water
 536 contents of both compartments weighted by their relative volume:

537

538 $\theta_f = \frac{V_2 \theta_2 + V_3 \theta_3}{V_2 + V_3}$, (32)

539

540 where the volumes of compartments (2) and (3) are calculated respectively as $V_2 = F_{vs} z_2$ and

541 $V_3 = F_{bs} (z_R - z_1) + F_{vs} (z_R - z_2)$. The stress function for the vegetated soil simply involves $\theta_{vs} =$
 542 θ_2 .

543

544 2.3.2 Capillary rise

545

546 The upward flow of groundwater to the root zone by capillary rise is driven by the soil
 547 hydraulic properties, the vertical gradient of water potential and the depth of the saturated
 548 zone (Maxwell and Miller, 2005; Vervoort and van der Zee, 2008), with high nonlinearities
 549 involved (Bogaart et al., 2008). When the water table is shallow, the increase in soil moisture

550 of the root zone induced by the upward flow from the saturated zone can directly influence
 551 the magnitude and seasonal course of evaporation (Guix-Hébrard et al., 2007; Soyulu et al.,
 552 2011). In the present work, the upward transfer of water by capillary rise (CR_3) from the
 553 saturated zone to reservoir (3) is estimated using a bulk form of Darcy's law, which considers
 554 the flow of water proportional to the difference of water potential and inversely proportional
 555 to the distance between reservoirs

$$557 \quad CR_3 = K_{G,3} \left(\frac{\Psi_{s,G} - \Psi_3}{\Delta z_{G,3}} \right), \quad (33)$$

558
 559 where $\Psi_{s,G}$ is the water potential of the saturated zone (Clapp and Hornberger, 1978), $\Delta z_{G,3}$ is
 560 the distance between the top of the saturated zone (z_G) and the bottom of reservoir (3) (z_R),
 561 and $K_{G,3}$ the soil hydraulic conductivity of the transition zone between z_G and z_R (Fig. 1). The
 562 water potential of unsaturated soil is the sum of pressure potential and gravitational potential
 563 taking the reference height at water table level $\Psi_3 = \Psi_{p,3} + (z_G - z_R)$. Pressure potential $\Psi_{p,3}$
 564 and hydraulic conductivity are determined as a function of soil water content θ_3 following
 565 Campbell (1974) and Clapp and Hornberger (1978)

$$567 \quad \Psi_{p,3}(\theta) = \frac{\Psi_{s,3}}{(\theta_3/\theta_{s,3})^{b_3}}, \quad (34)$$

568
 569 where the parameters $\Psi_{s,3}$, $\theta_{s,3}$ (water potential and soil water content for saturated
 570 conditions) and b_3 (a pore size distribution index) are given by Clapp and Hornberger (1978)
 571 according to soil properties. The unsaturated hydraulic conductivity of the transition zone
 572 ($K_{G,3}$) between the top of the water table and the bottom of reservoir (3) is a power function of
 573 soil moisture content of this transition zone between z_R and z_G (Campbell, 1974). Since this
 574 moisture content is a priori unknown, the same value as reservoir (3) is considered

$$576 \quad K_{G,3} = K_{s,3} \left(\frac{\theta_3}{\theta_{s,3}} \right)^{2b_3+3}, \quad (35)$$

577

578 $K_{s,3}$ is the hydraulic conductivity under saturated conditions. Finally, Darcy's law can be
579 rewritten in a bulk form as

580

$$581 \quad CR_3 = K_{G,3} \left[\left(\frac{1}{z_G - z_R} \right) \left(\Psi_{s,G} - \frac{\Psi_{s,3}}{(\theta_3 / \theta_{s,3})^{b_3}} \right) - 1 \right], \quad (36)$$

582

583 where $\Psi_{s,G}$ is the water potential of the saturated zone (Clapp and Hornberger, 1978), the
584 values of θ_3 being given by the soil water balance model at each time step.

585

586 **3. Experiment and model implementation**

587

588 **3.1 Study area**

589

590 The experiment took place in the vineyard watershed of the Peyne river, a tributary of
591 the Hérault river, located in the Languedoc-Roussillon region of southern France. The climate
592 is Mediterranean, with an average annual precipitation of 650 mm, mainly concentrated
593 during autumn and spring, and a dry summer season. Average annual reference evaporation is
594 1105 mm. Soil was a Cambisol (clayic) with a 2.3 to 2.5 m depth.

595 Measurements were carried out on flat vineyard (*Vitis vinifera* L.) of 13 hectares
596 located at 43.4739°N 3.3697°E, with an elevation of 42 m.a.s.l. The inter-row distance was
597 2.5 m and intra-row plant distance was 1 m. Vine canopy height and width was maintained at
598 1.5 m and 1 m, respectively, by regular thinning. The maximum value of vine LAI_f was 3. The
599 natural grass cover is characterized by a fractional area $F_{vs} = 0.3$ and $CLAI_{vs} = 2$ (Paré, 2011).

600

601 **3.2 Data collection**

602

603 Hourly values of solar radiation, air temperature, relative humidity, wind speed and
604 rainfall were continuously obtained from a CIMEL Enerco 400, following meteorological
605 standards, apart from wind speed (measured at 2 m height rather than 10 m for
606 agrometeorological purposes). This weather station was located 4.4 km east-northeast of the
607 vineyard.

608 Components of the energy balance were measured by using a portable micro
609 meteorological station equipped with a Young 81000 3D sonic anemometer (R.M. Young,

610 USA), a fast hygrometer KH20 (Campbell Inc., USA) and a net radiometer NRLite (Kipp-
611 Zonen, NLD), installed at 2.8 m above ground. An air temperature and relative humidity
612 probe HMP45C (Campbell Inc., USA) allowed correcting for the calibration drift of the
613 KH20. Three soil heat flux plates HFP01 (Hukseflux, NLD) were installed at 0.05 m below
614 the soil surface. This flux station was installed 10 times (3 in 2007, 7 in 2008) in the middle
615 of the vineyard, for 2-4 days periods. Raw data Eddy Covariance (EC) (wind speed
616 components, air temperature and humidity) were acquired at 20 Hz. Other data were acquired
617 at 1Hz and stored as 15 minutes averages.

618 Soil moisture data were obtained from a Vectra 503-DR CPN Neutron Probe (NP)
619 device. Soil moisture profile was sampled every 0.2 m between 0.2 and 2.5 m of soil depth.
620 This was performed biweekly and after significant rainfall events. The top 0.15 m layer was
621 monitored using a Soil Moisture Equipment TRASE 6050 Time Domain Reflectometry
622 sensor. Soil physical properties measured along the soil profile were averaged and weighted
623 by the corresponding horizon thickness in order to obtain a single value of actual water
624 content (θ), wilting point (θ_{wp}), field capacity (θ_{fc}), stone content (p) and constants for each
625 reservoir. Manual piezometric measurements conducted concurrently to the soil moisture
626 profiles demonstrated the absence of watertable in the first four meters.

627 Vines were monitored for height and leaf area was estimated during the period of
628 maximum growth using hemispherical photographs processed using the CAN_EYE software.
629 Further details on this experiment can be found in Galleguillos et al. (2011).

630

631 **3.3 Model forcing**

632

633 In context of developing a versatile and parsimonious SVAT model devoted to the
634 characterization of vineyard water consumption, the required forcing data are conventional
635 meteorological observations such as those collected during the experiment (air temperature,
636 relative humidity, global radiation, wind speed and daily-accumulated rainfall, see Section
637 3.2). Atmospheric radiation is estimated from available meteorological data through the
638 parameterization proposed in Appendix D, but direct measurements can be used when
639 existing.

640 The leaf area index of the vine foliage (LAI_f) is required as input variable in several
641 parameterizations (i.e. available energy components, air and surface resistances), whereby a
642 time series of LAI_f is required. The seasonal evolution of LAI_f is simulated as a function of
643 thermal time by means of a double logistic relationship (Clevers et al., 2002; Fisher et al.,

2006). In this approach, LAI_f rises up to a plateau and then decreases when senescence begins (Fig. 2k-2l). It is calculated as

$$LAI_f(TT) = (LAI_{f,max} - LAI_{f,min}) \left(\frac{1}{1 + e^{m_1 + m_2(TT - TT_1)}} - \frac{1}{1 + e^{m_3 + m_4(TT - TT_2)}} \right) + LAI_{f,min}, \quad (37)$$

with $LAI_{f,max}$ and $LAI_{f,min}$ the maximum and minimum values of LAI_f during the growing season, respectively; TT is the thermal time calculated with a daily time step

$$TT = \sum \max \left(\frac{T_{max} + T_{min}}{2} - T_b, 0 \right), \quad (38)$$

where T_{max} and T_{min} are the daily maximum and minimum temperatures ($^{\circ}C$), respectively, and T_b a base temperature below which plant growth is negligible, considered typically as $10^{\circ}C$ for grapevine (Winkler and Williams, 1939). In Eq. (37) m_1 and m_2 are fitting parameters that control the growth stage, m_3 and m_4 are those for the senescence stage, TT_1 and TT_2 represent empirical values that drive the beginning and ending of the vegetative cycle. The values of the parameters were obtained by applying a basic fitting procedure considering the vegetation data collected over the 2008 season: the value of $LAI_{f,max}$ and the observed dates of three foliage stages (beginning of growth, maximum growth and beginning of senescence). The thermal summation began from 01-March-2008 (taking $LAI_{f,min} = 0$) and the values found were: $TT_1 = 800$, $TT_2 = 2500$, $m_1 = 0.01$, $m_2 = 0.07$, $m_3 = 0.01$ and $m_4 = 0.05$.

The grass cover is assumed to be already green and covering at the beginning of the seasonal cycle and to be completely senescent if a dry spell of seven consecutive days without available soil water ($ASW_2 = 0$) occurs (Paré, 2011). When this event occurs, only bare soil evaporation is considered during the following days ($F_{vs} = 0$). Local observations suggest that the grass cycle restarts after the grape harvest.

3.4 Model calibration

As for most SVAT models, the correct implementation of the three-source model described above depends upon the appropriate specification of the controlling parameters. They are often difficult to obtain empirically by local fitting and a wide variation in their

675 values is found in the literature. Moreover, their transferability to different environmental
676 conditions should be handled with care at the risk of systematic errors.

677 In the present work, a total of 31 parameters have to be defined first. Given the wide
678 range of values found in the literature and the lack of local observations, a total of 16
679 parameters related to energy balance and surface resistances (listed in Table 1) were obtained
680 by calibration, whereas a total of 15 soil-related parameters were obtained by local
681 observation (soil profile description) or direct consultation of the literature in the case of
682 capillary rise equations (Table 2). The calibrated parameters were calculated by applying the
683 Multi-objective Calibration Iterative Procedure (MCIP) algorithm developed by Demarty et al.
684 (2004, 2005). This multi-criteria global calibration method is based on the minimization of a
685 cost function describing the model performance in relation to field observations. Thus,
686 starting from an initial uncertainty range for each parameter (Table 1), an iterative procedure
687 is carried out to reduce the feasible parameter space by optimization of model outputs against
688 observations. Bastidas et al. (1999), Gupta et al. (1999) and Demarty et al. (2004, 2005)
689 provide detailed description of this multi-objective calibration approach, and several works in
690 land-surface models calibration have used this stochastic method, namely Coudert et al.
691 (2006), Saux-Picart et al. (2009) and Guillevic et al. (2012).

692 In an algorithmic way, for each iteration, the MCIP method can be summarized as
693 follows: (1) based on local measurements and literature, the initial feasible parameter space is
694 defined (Table 1); (2) the parameter space is uniformly sampled and a set of Monte Carlo
695 random simulations is performed for each parameter combination (2000 in our case); (3) the
696 corresponding cost functions are calculated for every single simulation, in this case using the
697 root mean square errors (RMSE[†]) between model estimates and observed values; (4) using the
698 Pareto ranking approach, or a simple sorting when only one objective function is calculated,
699 the resulting cost function ensemble is partitioned into acceptable and non-acceptable
700 solutions according to a prescribed cost functions threshold; (5) a sensitivity analysis of
701 model parameters is performed based on the MOGSA algorithm (Bastidas et al., 1999), which
702 consists in carrying out the non-parametric test of Kolmogorov-Smirnov to statistically
703 compare the empirical cumulative distribution of model parameters between the acceptable
704 and non-acceptable solutions; and (6) the parameter space is contracted for those parameters
705 with significant differences between the two samples (i.e. sensitive parameters) found in (5),

† RMSE = $\sqrt{\sum_1^n (e_i - m_i)^2 / n}$, with e_i the estimated value and m_i the observed value at time step i

706 and then a new set of simulations is performed. Parameters found as no sensitive are left to
707 vary freely in the *a priori* uncertainty range of the precedent iteration. These steps are
708 executed iteratively (10 iterations in our case) in order to narrow the parameter range until an
709 optimized set of parameters is obtained.

710 In the present work, this methodology was applied to obtain an optimized set of
711 parameters belonging to the plant-atmosphere module (Table 1), soil parameters being set as
712 constant during the calibration procedure (Table 2). In this way, total latent heat flux was
713 simulated and the cost function (RMSE) was minimized for a total of eight selected days
714 where both evaporation and soil water content measurements were available. Initial soil water
715 content of the three reservoirs was set by correcting the first observed value by the cumulative
716 evaporation of the previous days.

717

718 **4. Results**

719

720 The simulation period is constrained by the data availability, comprising the growing
721 season from 25-July through 30-September in 2007 and from 10-April through 30-September
722 in 2008. The time series of meteorological data used for model forcing during the simulation
723 period are shown in Fig. 2a-2j. The time series of LAI_f obtained with Eq. (37) and $CLAI_{vs}$,
724 both used for model forcing, are shown in Fig. 2k-2l. Local information from growers
725 indicates that, given vineyard pruning, $LAI_{f,max}$ can be taken as the same for 2007 and 2008
726 seasons, so the same curve was used in both simulation periods. A contrasting soil water
727 recharge was observed during these two periods: the 2007 season was characterized by dryer
728 conditions, with 262 mm (versus 321 mm in 2008) of cumulated rainfall from April through
729 September. Furthermore, the fall and winter precipitations preceding the vineyard growing
730 seasons provided a lower load in 2007 than in 2008: 173 mm versus 306 mm from October to
731 March.

732 In the first part of this section, the values of the parameters obtained with the MCIP
733 algorithm are presented and analyzed. The second part addresses the validation of the diurnal
734 course of hourly evaporation derived from the surface energy balance module only, as forced
735 with measurements of net radiation and soil moisture. In the third part, the whole model,
736 including both the surface energy balance and the soil water balance, is validated on
737 simulations of water balance at a daily time step. Finally, the model versatility is explored by
738 analyzing the impact of capillary rise and vineyard structure on total evaporation and soil

739 water balance.

740

741 **4.1 Analyzing calibrated parameters**

742

743 The values of the parameters of the plant-atmosphere module inferred from the MCIP
744 algorithm are shown in Table 1. There are two types of parameters: a set of biophysical
745 parameters obtainable from measurements and another one corresponding to fitting empirical
746 coefficients. Checking the pertinence and accuracy of the first set of optimized values is
747 necessary. Very few references in the literature report measurements of these parameters for
748 vineyards.

749 The attenuation coefficient of the vineyard foliage for net radiation $c = 0.45$ was
750 obtained by the MCIP algorithm. In the literature there is a large range of values for this
751 parameter. Sene (1994) proposed $c = 0.68$ for a different type of vineyard grown in southern
752 Spain and characterized by free standing bushes with a higher aerial biomass. This value was
753 also used by Zhang et al. (2008) in China. The value $c = 0.38$ was obtained by Poblete-
754 Echeverria and Ortega-Farias (2009) and $c = 0.5$ by Ortega-Farias et al. (2007) for vineyards
755 in central Chile. These last values are closer to that found here ($c = 0.45$), likely due to a
756 higher similarity with the vineyards trained in trellis system for the same variety under
757 Mediterranean-type conditions.

758 The maximum stomatal conductance calculated by the MCIP algorithm was $g_{x,f} =$
759 $3.3 \times 10^{-3} \text{ m s}^{-1}$. This value is fairly realistic since it is within the range of values measured by
760 Winkel and Rambal (1990) ($1.25 \times 10^{-3} \text{ m s}^{-1}$), Lebon et al. (2003) ($2.86 \times 10^{-3} \text{ m s}^{-1}$), Zhang et
761 al. (2008) ($6.85 \times 10^{-3} \text{ m s}^{-1}$), Ortega-Farias et al. (2010) ($6.94 \times 10^{-3} \text{ m s}^{-1}$) and also close to the
762 daytime average value found by Ortega-Farias et al. (2007) on irrigated vineyard ($2.13 \times 10^{-3} \text{ m}$
763 s^{-1}). Also, Jones et al. (2002) found an average $g_{x,f} = 4.0 \times 10^{-3}$ between shaded and sunlit
764 leaves in irrigated vineyard. For the grass cover, its Mediterranean type can explain the lower
765 value retrieved for its maximal stomatal conductance $g_{x,vs}$ than the daytime average value of
766 Allen et al. (1989) ($g_{x,vs} = 1.0 \times 10^{-2} \text{ m s}^{-1}$).

767 The relatively large dispersion observed in the measured values of $g_{x,f}$ and c reveals
768 the difficulty to find adequate values for model parameters and justifies the use of a stochastic
769 approach. Conversely, a smaller variability is observed for vineyard albedo. The optimized
770 value $a_f = 0.24$ is close to those found by Sene et al. (1994) ($a_f = 0.27$), Pieri and Gaudillère
771 (2003) ($a_f = 0.2$) and Ortega-Farias et al. (2010) ($a_f = 0.19$). On the other hand, optimized
772 substrate albedos ($a_{bs} = 0.3$ and $a_{bs} = 0.25$) are very close to those often found in the literature

773 for dry and grassed soils (e.g. Idso et al., 1975; Grasser and van Babel, 1982; Davies, 2006).
774 The differences are ascribed to different substrate composition.

775 Finally, when dealing with soil heat flux estimation, the retrieved fraction β_{bs} for bare
776 soil is higher than β_{vs} for vegetated soil, which is in agreement with the thermal properties of
777 both covers.

778

779 4.2 Evaporation estimates

780

781 In this section, the evaporation model is evaluated alone, without being coupled with
782 the soil water balance module. Measurements of soil water content and net radiation are used
783 as input data for Eq. (20) and Eqs. (7) to (11), respectively, in order to evaluate the three-
784 source scheme itself, independently of its operational utilization on a seasonal basis. The
785 model performance in terms of simulated daily course of total evaporation is compared
786 against a set of EC measurements during the contrasting environmental conditions of 2007
787 and 2008, which constitutes an assessment of the residual calibration error. A comparison
788 between the SVAT model outputs and the set of hourly EC measurements is shown in Fig. 3,
789 including the agreement evaluation by using the root mean square error (RMSE), the bias
790 estimation (B^{\ddagger}) and the coefficient of determination (R^2). A quite reasonable agreement
791 between estimated and measured evaporation rates was obtained at the hourly timescale with
792 a high linear representation ($R^2 = 0.95$).

793 Fig. 4 shows the diurnal variation of evaporation simulated by the model compared to
794 EC data for eight distinct days. A good agreement is observed between the daily cycle of
795 model estimates and EC measurements in spite of a slight overestimation on 14-Jun-2008 and
796 a minor underestimation at the end of the 2008 season (09-Aug-2008). The strong soil water
797 content depletion during 2007 is evidenced through a significant reduction in λE_t (Figs. 4a-4c),
798 despite the almost constant LAI_f (Fig. 2k). In 2008, the initial growing period (Fig. 4d) is
799 characterized by the low foliage area of the vines ($LAI_f = 0.7 \text{ m}^2 \text{ m}^{-2}$), when λE_t emanates
800 mainly from bare and vegetated soils. When vine LAI_f increases, its transpiration increases
801 leading to maximum values of latent heat flux around 250 W m^{-2} (Figs. 4f-4g). During the
802 two periods shown in Figs. 4f and 4g, when vine foliage is fully developed (LAI_f close to 3),
803 the agreement between the two λE_t series is rather good. This period of the growing season
804 can be considered as the most important from an agricultural point of view, given the impact

$\ddagger B = \sum_1^n (e_i - m_i) / n$, with e_i the estimated value and m_i the observed value at time step i

805 of water stress on grape production (Schultz, 1996).

806

807 **4.3 Seasonal dynamics of water balance**

808

809 In this section, the evaporation model is coupled with the soil module to jointly
810 simulate the seasonal dynamics of total evaporation (E_t) and soil water content. E_t is obtained
811 from Eq. (4) using the simulated soil water content θ to solve Eq. (20). The water table being
812 fairly deep (down to 4 m) during the simulation period, the impact of capillary rise is
813 considered as negligible and the corresponding module is shutdown. In addition, the iterative
814 approach presented in Section 2.2.3 is used to obtain the net radiation. It yields relatively
815 good estimates, compared to measured values (RMSE = 46 W m⁻²; results not shown), but
816 with a slight overestimation, maybe explained by a higher load of atmospheric radiation
817 obtained by the scheme detailed in Appendix D, which certainly would have required a local
818 calibration (e.g. Lhomme et al., 2007).

819 An overall comparison between simulated and observed E_t and θ values for both
820 seasons is shown in Fig. 5a and 5b, respectively. The simulated value of θ is calculated as the
821 weighted mean of the water content of each reservoir. The evaporation results show a
822 relatively good agreement between model and EC data, with a regression slope close to 1, but
823 some overestimation is observed. A possible explanation is the method implemented for
824 estimating net radiation, which led to an overestimation of this input variable (bias = +21 W
825 m⁻² between 07:00 and 18:00 local time), and therefore an increase of available energy for
826 evaporation. The same comparison for θ (Fig. 5b) shows that very good estimates were
827 obtained for both contrasting seasons.

828 Fig. 6 shows the time series of modeled daily evaporation and soil water content
829 during the two seasonal simulations. In general, the agreement between the simulated curves
830 and the observed data is rather good. A strong temporal decay in both evaporation and θ
831 characterizes the 2007 season, as a response of very low precipitations (Fig. 2i). For the 2008
832 season (Fig. 6b), the evaporation experiences a seasonal course that agree quite well with EC
833 measurements. The seasonal evolution follows the seasonal shape of the meteorological
834 forcing and foliage development. Concerning soil water content (θ), a slight increase induced
835 by a relatively low evaporative demand and by several rainfall events (till mid-June 2008, see
836 Fig. 2j) is followed by a progressive decrease until the end of the growing season (Fig. 6d).
837 During the last part of the period (September 2008), overestimated values of θ are obtained
838 with the model, which could receive the following explanation. The dry conditions and the

839 absence of grass cover during the last part of the growing season have induced soil crusting
840 which reduces the infiltration capacity and enhances surface runoff. Consequently, the strong
841 rainfall event just before the last measurement days (Fig. 2j), which potentially could have
842 involved important water filling for the soil, may have been lost by runoff. This phenomenon
843 was observed by Lebon et al. (2003) in the same region and also by Gaudin et al. (2010) in an
844 inter-cropping vineyard.

845

846 **4.4 Analysis of model predictions**

847

848 In order to illustrate model versatility, some static simulations were undertaken in
849 order to examine the SVAT model under different configurations of the vineyard system and
850 to explore the impact of crop characteristics on evaporation.

851

852 4.4.1 Impact of capillary rise

853

854 A simulation with constant boundary conditions was performed in order to quantify
855 the magnitude of the water flow from the saturated zone into reservoir (3) (CR_3). In our
856 formulation CR_3 varies as a function of the saturated zone depth (z_G) and the soil water
857 content of reservoir (3) (θ_3). The same soil texture (clay loam) for reservoir (3) and the
858 transition zone between z_G and z_R is considered and the corresponding values of hydraulic
859 parameters taken from Clapp and Hornberger (1978) are shown in Table 2. Fig. 7 shows the
860 predicted values of CR_3 as a function of θ_3 and of the distance between the root zone and the
861 water table $z_G - z_R$. As can be anticipated, capillary rise (CR_3 value) decreases with the
862 distance ($z_G - z_R$) and increases with the soil water content θ_3 in relation with the hydraulic
863 conductivity $K_{G,3}$. Although it was not possible to confront these values with field
864 measurements, they are within the range of values obtained by several authors from similar or
865 more complex approaches of capillary rise (e.g. Raes and Deproost, 2003; Bogaart et al. 2008;
866 Vervoort et al. 2008). Our results are realistic and confirm the possible use of the capillary
867 rise module when the water table is shallow.

868

869 4.4.2 Impact of vineyard structure on evaporation rate

870

871 In our approach, the geometry of the grassed vineyard system can be characterized by
872 the distance between rows and the relative proportion of grass (F_{vs}) and bare soil (F_{bs}). In

873 order to estimate the impact of foliage surface proportion on vineyard evaporation, the
 874 concept of clumped leaf area index ($CLAI_f$) is used (defined as the leaf area per unit area of
 875 substrate covered by the foliage): $LAI_f = F_f CLAI_f$, where F_f is the proportion of soil surface
 876 occupied by the vine canopy. F_f depends on the width of the vine row (w_r) and on that of the
 877 inter-row (w_i), and can be expressed as

$$879 \quad F_f = \frac{w_r}{w_r + w_i} = \frac{1}{1 + w_i / w_r}. \quad (39)$$

880
 881 Inter-row width w_i is varied maintaining $CLAI_f$ and w_r fixed: 2.5 and 1 m respectively. In this
 882 way, total evaporation is simulated as a function of w_i and hence LAI_f using Eq. (39). Standard
 883 values of meteorological and soil variables were considered: $R_n = 400 \text{ W m}^{-2}$, $T_a = 25 \text{ }^\circ\text{C}$,
 884 $D_a = 10 \text{ hPa}$, $u_a = 2 \text{ m s}^{-1}$, $R_g = 600 \text{ W m}^{-2}$, $\theta_f = 0.3$, $\theta_{vs} = 0.25$, $\theta_{bs} = 0.25$. Secondly, the
 885 proportion of vegetated soil F_{vs} (and consequently F_{bs}) is varied between 0 (bare soil only)
 886 and 1 (grassed soil only). The model is run by considering the combined effect of w_i and F_{vs}
 887 variations on total evaporation E_t , all other conditions being kept constant. The results of this
 888 simulation are shown in Fig. 8: for $F_{vs} = 0.3$ (our experimental dataset) a decrease in E_t of
 889 about 0.02 mm h^{-1} is estimated when the distance between rows w_i varies from 0.5 to 4 m. For
 890 $w_i = 2 \text{ m}$, E_t increases of about 0.1 mm h^{-1} when passing from fully bare ($F_{vs} = 0$) to fully
 891 grassed soil ($F_{vs} = 1.0$), suggesting a higher sensitivity to grass cover.

892

893 **5. Discussion**

894

895 A quite good performance of the proposed SVAT model was obtained in representing
 896 the seasonal water balance. Model estimates of total evaporation are quite good when
 897 considering the surface energy balance module alone (Fig. 3), forced with measured net
 898 radiation and soil moisture. They are less accurate when considering the coupling between
 899 surface energy balance and soil water balance (Fig. 5). This is ascribed to the fact that net
 900 radiation and soil moisture are simulated and not measured. Certainly, the parameterization
 901 adopted for foliage surface resistance is critical. Indeed, the model was found very sensitive to
 902 the stress function f_3 of Eq. (20) involving soil moisture (θ). In addition, the maximum leaf
 903 conductance of grapevine $g_{x,f}$ (Eq. (17)) was found to be highly variable in the literature. It
 904 might also vary in time as a function of phenological stage and environmental conditions, so

905 that the use of a single value over the whole season might be inappropriate. Previous works
906 have shown that parameter sensitivity can vary for different periods (Demarty et al., 2005;
907 Guillevic et al., 2012) and that a period-specific calibration associated with the seasonal
908 variability in vegetation properties or rainfall should be preferable (Coron et al., 2012;
909 Gharari et al., 2013).

910 The equations used for aerodynamic resistances (Appendix C) are very common in
911 micrometeorology but they could be a source of uncertainty. Indeed, given the influence of
912 vineyard geometry on wind flow within and above the foliage, there is a gap in the current
913 parameterizations of surface aerodynamic properties of crop canopies structured in rows. In
914 this sense, the influence of wind direction and row orientation has been reported in the
915 literature. For the case of vineyards, a significant increase in drag coefficient was found by
916 Hicks (1973) and a larger turbulent intensity by Weiss and Allen (1976) when wind flows
917 perpendicular to the rows. Also, important differences were found by Riou et al. (1987) for
918 vineyard aerodynamic parameters (z_0 and d) as a function of wind direction and row
919 orientation, and variations in measured daytime aerodynamic resistance were found by Padro
920 et al. (1994) for different wind directions likely due to variations in z_0 . Recently, using Large
921 Eddy Simulation under neutral conditions, a major channeling effect between the vine rows
922 was described by Chahine et al. (2014) for row-parallel wind, increasing the spatial variability
923 in vertical wind profile and decreasing the value of aerodynamic parameters such as z_0 and d
924 in relation to normal and diagonal flow. They concluded that this effect may be more
925 pronounced under unstable conditions, which might be expected in Mediterranean regions
926 during the growing season. These points raise the challenge of improving the current
927 parameterizations of aerodynamic resistances including wind direction effects.

928 Uncertainties associated with R_n estimates and LAI_f simulations also play an important
929 role on the partition of available energy and on surface and aerodynamic resistances. More
930 complex models than Beer's law can be found in the literature for canopy radiative transfer
931 (Taconet et al., 1986; Braud et al., 1995). Lebon et al. (2003) stressed that a better partitioning
932 of incoming solar radiation between vines and substrate is obtained by using the model of
933 Riou et al. (1989) which involves vineyard geometrical properties. This model, only designed
934 for shortwave radiation, was later developed by Pieri (2010a, 2010b) for long-wave radiation
935 partitioning. For the specific case of row-growing crops, a comprehensive model for radiative
936 transfer and partition (short- and long-wave radiation) was recently proposed by Colaizzi et al.
937 (2012a, 2012b). Unfortunately, given the data requirements of these radiative models, their
938 implementation is rather difficult considering the scope of the present work.

939 A better representation of water stress and its impact on gas exchanges might be
940 addressed by taking into account the mechanisms responsible for variations in soil water
941 distribution and root water uptake along the profile (e.g. Tuzet et al., 2003; Amenu and
942 Kumar, 2008; Siqueira et al., 2008; Volpe et al., 2013). Certainly the simplified approach
943 adopted here represents a source of uncertainty to the model, especially in relation with vine
944 roots depth, their distribution and their impacts on soil moisture dynamics. However, the
945 inclusion of soil profiles into the soil water balance module would have significantly altered
946 the parsimonious nature of the model, and therefore its possible use at the regional extent.

947 Finally, it is clear that assuming a complete infiltration of rainfall can lead to some
948 discrepancies between model outputs and observations after strong rainfall events, such as the
949 one registered at the beginning of September 2008 (Figs. 2j, 6d). But the inclusion of runoff
950 into the soil water budget is a quite complex issue to solve in a one-dimensional approach.
951 The improvement of this component requires considering the horizontal heterogeneities in
952 soil physical properties responsible for horizontal transfers and could be carried out by
953 coupling SVAT models with spatially-distributed hydrological models (e.g. Bouilloud et al.
954 2010).

955

956 **6. Concluding remarks**

957

958 In this work, the seasonal pattern of evaporation from a grassed Mediterranean
959 vineyard was modeled by coupling an evaporation formulation together with a reservoir-type
960 soil water balance model. The evaporation formulation is based on a three-source model,
961 recently revisited by Lhomme et al. (2012), where some adaptations have been made in order
962 to use standard meteorological data as direct inputs to the model. This approach provides
963 realistic estimates of the component evaporations emanating from the three sources (main
964 foliage, grassed and bare soil) and allows the seasonal dynamics of soil moisture to be
965 correctly simulated. A good agreement was obtained when the seasonal course of total
966 evaporation and soil moisture simulations were compared against ground based references
967 during two contrasting seasons in terms of available soil water. Neglecting runoff, however,
968 can lead to some discrepancy after strong rainfall events on dry soil: soil crusting promotes
969 runoff and lower soil moisture recharge. This imposes limitations to the application of the
970 model and further investigation should focus on the coupling with distributed hydrological
971 models.

972 The model versatility can be used to explore the impact of the grassed vineyard

973 geometry on evaporation throughout the season and for different climate conditions. The
974 static simulations performed suggest that a significant impact should be expected when the
975 distance between vine rows and the fraction of grassed soil are modified.

976 Apart from the aforementioned limitations regarding the model performance,
977 uncertainties arise from the fact that a large number of parameters should be defined for the
978 controlling factors. This difficulty has been addressed by applying an optimization procedure
979 to find the optimal values of these parameters. However, these values can vary in relation
980 with grapevine phenological phases and could be improved by testing a larger number of
981 model outputs against measurements of energy and water balance.

982 Finally, another contribution of this parsimonious model is its potential use to estimate
983 water budget components at regional scale using remotely sensed data. The energy balance-
984 based evaporation formulation allows one to derive surface composite temperature which can
985 be compared to the satellite estimate of the corresponding radiometric temperature. Different
986 approaches have been developed to include this temperature into SVAT models through data
987 assimilation schemes in order to obtain energy balance components (Coudert et al., 2006;
988 Caparrini et al. 2008; Sini et al., 2008) or soil moisture estimates (Jones et al., 1998; Crow et
989 al., 2008).

990

991

992 **Acknowledgements**

993

994 This study was partly supported by the French Centre National d'Etudes Spatiales
995 (CNES/TOSCA) and by the European Commission's Seventh Framework Programme
996 (FP7/2007-2013) through the 'Research Infrastructures' action under ExpeER project (grant
997 agreement n°262060). The first author acknowledges CONICYT-Chile for the doctoral grant.
998 The constructive comments and suggestions from three anonymous reviewers are highly
999 appreciated.

1000

1001 **Appendix A. Coefficients of the evaporation formulation (Eq. (4))**

1002

1003 $P_f = r_a R_{vs} R_{bs} / DE,$ (A1)

1004

1005 $P_{vs} = r_a R_f R_{bs} / DE,$ (A2)

1006

1007 $P_{bs} = r_a R_f R_{vs} / DE,$ (A3)

1008

1009 with DE written as

1010

1011 $DE = R_f R_{vs} R_{bs} + R_f R_{vs} R_a + R_f R_{bs} R_a + R_{vs} R_{bs} R_a,$ (A4)

1012

1013 with the coefficients R_i being defined as

1014

1015 $R_f = r_{s,f} + \left(n + \frac{\Delta}{\gamma} \right) r_{a,f,h},$ (A5)

1016

1017 $R_{vs} = r_{s,vs} + \left(1 + \frac{\Delta}{\gamma} \right) r_{a,vs},$ (A6)

1018

1019 $R_{bs} = r_{s,bs} + \left(1 + \frac{\Delta}{\gamma} \right) r_{a,bs},$ (A7)

1020

1021 $R_a = r_a \left(1 + \frac{\Delta}{\gamma} \right).$ (A8)

1022

1023

1024 **Appendix B: Expressing the component surface temperatures**

1025

1026 Component surface temperatures T_i ($i = f, vs, bs$) are obtained by solving the energy
1027 balance for the three sources. The corresponding available energy (A_i) is equal to the sum of

1028 latent and sensible heat fluxes:

1029

$$1030 \quad A_i = \frac{\rho c_p}{\gamma} \frac{[e^*(T_i) - e_m]}{r_{s,i} + r_{a,i,v}} + \rho c_p \frac{T_i - T_m}{r_{a,i,h}}, \quad (\text{B1})$$

1031

1032 $r_{a,i,v}$ and $r_{a,i,h}$ representing the air resistances respectively for water vapor and sensible heat,

1033 T_m and e_m the air temperature and air vapor pressure at canopy source height (z_m), and $e^*(T_i)$

1034 the saturated vapor pressure at T_i . After linearizing $e^*(T_i) - e^*(T_m)$, Eq. (B1) is rewritten as:

1035

$$1036 \quad A_i = \frac{\rho c_p}{\gamma} \frac{[\Delta(T_i - T_m) + D_m]}{r_{s,i} + r_{a,i,v}} + \rho c_p \frac{T_i - T_m}{r_{a,i,h}}. \quad (\text{B2})$$

1037

1038 After some algebra and taking into account that $r_{a,i,v} = n r_{a,i,h}$, surface temperature can

1039 be expressed as:

1040

$$1041 \quad T_i - T_m = \frac{(nr_{a,i,h} + r_{s,i})A_i / \rho c_p - D_m / \gamma}{n + \Delta / \gamma + r_{s,i} / r_{a,i,h}}, \quad (\text{B3})$$

1042

1043 with $n = 2$ for the foliage ($i = f$) and $n = 1$ for the substrate components ($i = vs, bs$), T_m being

1044 obtained by $T_m = T_a + H r_a / \rho c_p$.

1045

1046

1047 **Appendix C: Formulations of aerodynamic resistances**

1048

1049 The aerodynamic resistance above the canopy (r_a) is calculated using the equation that

1050 takes into account the stability correction functions for wind (Ψ_m) and temperature (Ψ_h)

1051 (Brutsaert, 1982):

1052

$$1053 \quad r_a = \left(\frac{1}{k^2 u_a} \right) \left[\ln \left(\frac{z_r - d}{z_0} \right) - \Psi_h \left(\frac{z_r}{L} \right) \right] \left[\ln \left(\frac{z_r - d}{z_0} \right) - \Psi_m \left(\frac{z_r}{L} \right) \right], \quad (\text{C1})$$

1054

1055 where u_a is the wind speed at reference height z_r and L is the Monin-Obukhov length. The

1056 canopy roughness length z_0 is determined following Choudhury and Monteith (1988):

1057

$$1058 \quad z_0 = \begin{cases} \bar{z}_{0,s} + 0.3z_h X^{0.5}, & \text{if } 0 < X \leq 0.2 \\ 0.3z_h \left(1 - \frac{d}{z_h}\right), & \text{if } 0.2 < X < 1.5 \end{cases} \quad (\text{C2})$$

1059

1060 where $X = c_d LAI_f$, with $c_d = 0.2$ the mean drag coefficient assumed to be uniform within the

1061 canopy and $\bar{z}_{0,s}$ the average value of substrate roughness length (= 0.0125 m). Following the

1062 same authors the displacement height d is expressed by

1063

$$1064 \quad d = 1.1z_h \ln(1 + X^{0.25}), \quad (\text{C3})$$

1065

1066 where z_h is the mean canopy height (vineyard).

1067 The aerodynamic resistance between the substrate ($i = vs$ and bs) and the canopy

1068 source height ($d + z_0$) is calculated (per unit area of substrate) as (Choudhury and Monteith,

1069 1988)

1070

$$1071 \quad r_{a,i}^1 = \frac{z_h \exp(\alpha_w)}{\alpha_w K(z_h)} \left\{ \exp\left[-\alpha_w z_{0,i}/z_h\right] - \exp\left[-\alpha_w (d + z_0)/z_h\right] \right\}, \quad (\text{C4})$$

1072

1073 where z_h is the height of the main foliage (vineyard), $\alpha_w = 2.5$ (dimensionless), $z_{0,i}$ the

1074 roughness length for momentum of vegetated ($z_{0,vs} = 0.015$ m) and bare soil ($z_{0,bs} = 0.010$ m).

1075 $K(z_h)$ is the value of eddy diffusivity at canopy height, obtained by

1076

$$1077 \quad K(z_h) = \frac{k^2 u_a (z_h - d)}{\ln\left[(z_r - d)/z_0\right]}. \quad (\text{C5})$$

1078

1079 Foliage bulk boundary later resistance for sensible heat is expressed as (Choudhury

1080 and Monteith, 1988)

1081

$$1082 \quad r_{a,f,h} = \frac{\alpha_w [w/u(z_h)]^{1/2}}{4\alpha_0 LAI_f [1 - \exp(-\alpha_w/2)]}, \quad (\text{C6})$$

1083

1084 where w is leaf width (0.01 m), α_0 is a constant equal to 0.005 (in $\text{m s}^{-1/2}$) and $u(z_h)$ is the
1085 wind speed at z_h , obtained by

1086

$$1087 \quad u(z_h) = u_a \frac{\ln\left[\frac{(z_h - d)/z_0}{(z_r - d)/z_0}\right]}{\ln\left[\frac{(z_r - d)/z_0}{(z_0 - d)/z_0}\right]}. \quad (\text{C7})$$

1088

1089

1090 **Appendix D: Estimating atmospheric radiation**

1091

1092 The incoming longwave radiation (R_{atm}) was parameterized using a formulation
1093 including both the effects of clear and cloudy sky conditions on R_{atm} . Several methods have
1094 been developed to estimate this component of radiative budget, which are often based on
1095 empirical formulations depending on air temperature and humidity (e.g. Brunt, 1932; Idso and
1096 Jackson, 1969; Duarte et al., 2006). In the present study the Brutsaert (1975) formulation was
1097 used to calculate the clear sky atmospheric radiation which is expressed as

1098

$$1099 \quad R_{atm,c} = a_1 (e_a/T_a)^{b_1} \sigma T_a^4, \quad (\text{D1})$$

1100

1101 e_a is the actual vapor pressure (Pa), and a_1 and b_1 are constant with values 1.24 and 0.14,
1102 respectively. Under cloudy sky conditions the fractional cover should be used, but this
1103 measure is very difficult to obtain in operational terms using conventional weather stations.
1104 Crawford and Duchon (1999) showed that a good estimation of sky condition could be
1105 obtained using the ratio R_g/R_0 between the measured solar irradiance (R_g) and the clear-sky
1106 irradiance (R_0). R_0 was obtained as a fraction of the extraterrestrial radiation (R_{ext} , the
1107 theoretical solar radiation at the top of the atmosphere) using the formulation proposed by
1108 Allen et al. (1998):

1109

$$1110 \quad R_0 = R_{ext} (0.75 + 2 \times 10^{-5} Z), \quad (\text{D2})$$

1111

1112 with Z the site elevation (masl). So, considering both clear and cloudy skies conditions the
1113 downwelling longwave atmospheric radiation is estimated as (Crawford and Duchon, 1999)

1114

$$1115 \quad R_{atm} = R_{atm,c} (R_g / R_0) + (1 - R_g / R_0) \sigma T_a^4. \quad (D3)$$

1116

1117 Since during nighttime the ratio R_g / R_0 cannot be calculated, Eq. (D3) was computed using

1118 the last value of R_g / R_0 during the previous afternoon (e.g. Lhomme et al., 2007).

1119

1120 **References**

1121

1122 Allen, R.G., Jensen, M.E., Wright, J.L., Burman, R.D., 1989. Operational estimates of
1123 reference evapotranspiration. *Agron. J.* 81,650-662.

1124 Allen, R.G., Pereira, L.S., Raes, D., Smith, M., 1998. *Crop evapotranspiration. FAO Irrigation
1125 and Drainage Paper 56, Rome.*

1126 Amenu, G.G., Kumar, P., 2008. A model for hydraulic redistribution incorporating coupled
1127 soil-root moisture transport. *Hydrol. Earth Syst. Sci.* 12, 55-74.

1128 Anderson, M.A., Norman, J.M., Diak, G.R., Kustas, W.P., Mecikalski, J.R., 1997. A two-
1129 source time-integrated model for estimating surface fluxes using thermal infrared remote
1130 sensing. *Remote Sens. Environ.* 60, 195-216.

1131 Anderson, M.C., Norman, J.M., Kustas, W.P., Li, F., Prueger, J.H., Mecikalski, J.R., 2005.
1132 Effects of vegetation clumping on two-source model estimates of surface energy fluxes
1133 from an agricultural landscape during SMACEX. *J. Hydrometeorol.* 6, 892-909.

1134 Bastidas, L.A., Gupta, H.V., Sorooshian, S., Shuttleworth, W.J., Yang, Z.L., 1999. Sensitivity
1135 analysis of a land surface scheme using multicriteria methods. *J. Geophys. Res.* 104,
1136 19481– 19490.

1137 Bogaart, P.W., Teuling, A.J., Troch, P.A., 2008. A state-dependent parameterization of
1138 saturated-unsaturated zone interaction. *Water Resour. Res.* 44, 1-10.

1139 Bouilloud, L., Chancibault, K., Vincendon, B., Ducrocq, V., Habets, F., Saulnier, G.-M.,
1140 Anquetin, S., Martin, E., Noilhan, J., 2010. Coupling the ISBA land surface model and
1141 the TOPMODEL hydrological model for Mediterranean flash-flood forecasting:
1142 description, calibration, and validation. *J. Hydrometeorol.* 11, 315-333.

1143 Boulet, G., Chehbouni, G., Braud, I., Vauclin, M., 1999. Mosaic versus dual source
1144 approaches for modelling the surface energy balance of a semi-arid land. *Hydrol. Earth
1145 Syst. Sci.* 3, 247-258.

1146 Boulet, G., Chehbouni, A., Braud, I., Vauclin, M., Haverkamp, R., Zammit, C., 2000. A
1147 simple water and energy balance model designed for regionalization and remote sensing
1148 data utilization. *Agr. Forest Meteorol.* 105, 117-132.

1149 Braud, A.C., Dantas-Antonino, M., Vauclin, J.L., Thony, Ruelle, P., 1995. A simple soil-
1150 plant-atmosphere transfer model (SiSPAT) development and field verification. *J. Hydrol.*
1151 166, 213-250.

1152 Brenner, A.J., Incoll, L.D., 1997. The effect of clumping and stomatal response on
1153 evaporation from sparsely vegetated shrublands. *Agr. Forest Meteorol.* 84, 87-205.

- 1154 Brunt, D., 1932. Notes on radiation in the atmosphere. Q. J. Roy. Meteor. Soc. 58, 389-420.
- 1155 Brutsaert, W.H., 1975. On a derivable formula for long-wave radiation from clear skies. Water
1156 Resour. Res. 11, 742-744.
- 1157 Brutsaert, W., 1982. Evaporation into the Atmosphere. Reidel Publishing Company,
1158 Dordrecht, 299 pp.
- 1159 Campbell, G.S., 1974. A simple method for determining unsaturated hydraulic conductivity
1160 from moisture retention data. Soil Sci. 177, 311-314.
- 1161 Caparrini, F., Castelli, F., Entekhabi, D., 2004. Estimation of surface turbulent fluxes through
1162 assimilation of radiometric surface temperature sequences. J. Hydrometeorol. 5, 145-159.
- 1163 Celette, F., Wery, J., Chantelot, E., Celette, J., Gary, C., 2005. Belowground interactions in a
1164 vine (*Vitis vinifera* L.)-tall fescue (*Festuca arundinacea* Shreb.) intercropping system:
1165 water relations and growth. Plant Soil. 276, 205-217.
- 1166 Celette, F., Gaudin, R., Gary, C., 2008. Spatial and temporal changes to the water regime of a
1167 Mediterranean vineyard due to the adoption of cover cropping. Eur. J. Agron. 29, 153-162.
- 1168 Celette, F., Ripoche, A., Gary, C., 2010. WaLIS – A simple model to simulate water
1169 partitioning in a crop association: The example of an intercropped vineyard. Agr. Water
1170 Manage. 97, 1749-1759.
- 1171 Centinari, M., Poni, S., Intrigliolo, D.S., Dragoni, D., Lakso, A.N., 2012. Cover crop
1172 evapotranspiration in a northeastern US Concord (*Vitis labruscana*) vineyard. Aust. J.
1173 Grape Wine Res. 18, 73-79.
- 1174 Chahine, A., Dupont, S., Sinfort, C., Brunet, Y., 2014. Wind-flow dynamics over vineyards.
1175 Bound.-Lay. Meteorol. DOI 10.1007/s10546-013-9900-4
- 1176 Choudhury, B.J., Monteith, J.L., 1988. A four-layer model for the heat budget of
1177 homogeneous land surfaces. Q. J. Roy. Meteor. Soc. 114, 373-398.
- 1178 Choudhury, B.J., 1989. Estimating evaporation and carbon assimilation using infrared
1179 temperature data: vistas in modeling. In G. Asrar (ed.), Theory and applications of optical
1180 remote sensing. Wiley, New York.
- 1181 Choudhury, B.J., Idso, S.B., Reginato, R.G., 1987. Analysis of an empirical model for soil
1182 heat flux under a growing wheat crop for estimating evaporation by an infrared-
1183 temperature based energy balance equation. Agr. Forest Meteorol. 39, 283-297.
- 1184 Clapp, R.B., Hornberger, G.M., 1978. Empirical equations for some soil hydraulic properties.
1185 Water Resour. Res. 14, 601-604.
- 1186 Clevers, J.G.P.W., Vonder, O.W., Jongschaap, R.E.E., Desprats, J., King, C., Prévot, L.,
1187 Ruguier, N., 2002. Using SPOT data for calibrating a wheat growth model under

1188 mediterranean conditions. *Agronomie* 22, 687-694.

1189 Colaizzi, P.D., Evett, S.R., Howell, T.A., Li, F., Kustas, W.P., Anderson, M.C., 2012a.
 1190 Radiation model for row crops: I. Geometric view factors and parameter optimization.
 1191 *Agron. J.* 104, 225-240.

1192 Colaizzi, P.D., Scwartz, R.C., Evett, S.R., Howell, T.A., Gowda, P.H., Tolck, J.A., 2012b.
 1193 Radiation model for row crops: II. Model evaluation. *Agron. J.* 104, 241-255.

1194 Coron, L., Andréassian, V., Perrin, C., Lerat, J., Vaze, J., Bourqui, M., Hendrickx, F., 2012.
 1195 Crash testing hydrological models in contrasted climate conditions: An experiment on
 1196 216 Australian catchments. *Water Resour. Res.* 48, W05552,
 1197 doi:10.1029/2011WR011721

1198 Coudert, B., Ottlé, C., Boudevillain, B., Demarty, J., Guillevic, P., 2006. Contribution of
 1199 thermal infrared remote sensing data in multiobjective calibration of a dual-source SVAT
 1200 model. *J. Hydrometeorol.* 7, 404-420.

1201 Crawford, T.M., Duchon, C.E., 1999. An improved parameterization for estimating effective
 1202 atmospheric emissivity for use in calculating daytime downwelling longwave radiation. *J.*
 1203 *Appl. Meteorol.* 38, 474-480.

1204 Crow, W.T., Kustas, W.P., Prueger, J.H., 2008. Monitoring root-zone soil moisture through
 1205 the assimilation of a thermal remote sensing-based soil moisture proxy into a water
 1206 balance model. *Remote Sens. Environ.* 112, 1268-1281.

1207 Davies, J.A., 2006. A note on the relationship between net radiation and solar radiation. *Q. J.*
 1208 *Roy. Meteor. Soc.* 93, 109-115.

1209 Demarty, J., Ottlé, C., Braud, I., Olioso, A., Frangi, J.P., Bastidas, L.A., Gupta, H.V., 2004.
 1210 Using a multiobjective approach to retrieve information on surface properties used in a
 1211 SVAT model. *J. Hydrol.* 287, 214-236.

1212 Demarty, J., Ottlé, C., Braud, I., Olioso, A., Frangi, J.P., Gupta, H.V., Bastidas, L.A., 2005.
 1213 Constraining a physically based Soil-Vegetation-Atmosphere Transfer model with surface
 1214 water content and thermal infrared brightness temperature measurements using a
 1215 multiobjective approach. *Water Resour. Res.* 41, W01011, doi:10.1029/2004WR003695.

1216 Duarte, H.F., Dias, N.L., Maggionto, S.R., 2006. Assessing daytime downward long-wave
 1217 radiation estimates for clear and cloudy skies in Southern Brazil. *Agr. Forest Meteorol.*
 1218 139, 171-181.

1219 Fisher, J.I., Mustard, J.F., Vadeboncoeur M.A., 2006. Green leaf phenology at Landsat
 1220 resolution: scaling from the field to the satellite. *Remote Sens. Environ.* 100, 265-279.

1221 Galleguillos, M., Jacob, F., Prévot, L., French, A., Lagacherie, P., 2011. Comparison of two

1222 temperature differencing methods to estimate daily evapotranspiration over a
1223 Mediterranean vineyard watershed from ASTER data. *Remote Sens. Environ.* 115, 1326-
1224 1340.

1225 Gaudin, R., Celette, F., Gary, C., 2010. Contribution of runoff to incomplete off season soil
1226 water refilling in a Mediterranean vineyard. *Agr. Water Manage.* 97, 1534-1540.

1227 Gharari, S., Hrachowitz, M., Fenicia, F., Savenije, H.H.G., 2013. An approach to identify
1228 time consistent model parameters: sub-period calibration. *Hydrol. Earth Syst. Sci.* 17,
1229 149-161.

1230 Graser, E.A., Van Babel, C.H.M., 1982. The effect of soil moisture upon soil albedo. *Agr.*
1231 *Meteorol.* 27, 17-26.

1232 Guillevic, P.C., Privette, J.L., Coudert, B., Palecki, M.A., Demarty, J., Otlé, C., Augustine,
1233 J.A., 2012. Land Surface Temperature product validation using NOAA's surface climate
1234 observation networks - scaling methodology for the Visible Infrared Imager Radiometer
1235 Suite (VIIRS). *Remote Sens. Environ.* 124, 282-298.

1236 Guix-Hébrard, N., Voltz, A., Trambouze, W., Garnier, F., Gaudillère, J.P., Lagacherie, P.,
1237 2007. Influence of watertable depths on the variation of grapevine water status at the
1238 landscape scale. *Eur. J. Agron.* 27, 187-196.

1239 Gupta, H.V., Bastidas, L.A., Sorooshian, S., Shuttleworth, W.J., Yang, Z.L., 1999. Parameter
1240 estimation of a land surface scheme using multicriteria methods. *J. Geophys. Res.* 104,
1241 19491-19503.

1242 Hicks, B.B., 1973. Eddy flux over a vineyard. *Agric. For. Meteorol.* 12, 203-215.

1243 Holland, S., Heitman, J.L., Howard, A., Sauer, T.J., Giese, W., Ben-Gal, A., Agam, N., Kool,
1244 D., Havlin, J., 2013. Micro-Bowen ratio system for measuring evapotranspiration in a
1245 vineyard interrow. *Agric. Forest Meteorol.* 177, 93-100.

1246 Idso, S.B., Jackson, R.D., 1969. Thermal radiation from the atmosphere. *J. Geophys. Res.* 74,
1247 5397-5403.

1248 Idso, S.B., Jackson, R.D., Reginato, R.J., Kimball, B.A., Nakayama, F.S., 1975. The
1249 dependence of bare soil albedo on soil water content. *J. Appl. Meteorol.* 14, 109-113.

1250 Jarvis, P.G., 1976. The interpretation of leaf water potential and stomatal conductance found
1251 in canopies in the field. *Phil. Trans. Roy. Soc. Lond. B.* 273, 593-610.

1252 Jones, A.S., Guch, I.C., Vonder Haar, T.H., 1998. Data assimilation of satellite-derived
1253 heating rates as proxy surface wetness data into a regional atmospheric mesoscale model.
1254 Part I: Methodology . *Mon. Wea. Rev.* 126, 634-645.

1255 Jones, H.G., Stoll, M., Santos, T., de Sousa, C., Chaves, M.M., Grant, O.M., 2002. Use of

1256 infrared thermography for monitoring stomatal closure in the field: application to
1257 grapevine. *J. Exp. Bot.* 53 (378), 2249-2260.

1258 Kustas, W.P., Zhan, X., Schmugge, T.J., 1998. Combining optical and microwave remote
1259 sensing for mapping energy fluxes in a semiarid watershed. *Remote Sens. Environ.* 64,
1260 116-131.

1261 Lebon, E., Dumas, V., Pieri, P., Schultz, H.R., 2003. Modelling the seasonal dynamics of the
1262 soil water balance of vineyards. *Funct. Plant Biol.* 30, 699-710.

1263 Lhomme, J.P., Chehbouni, A., 1999. Comments on dual-source vegetation-atmosphere
1264 transfer models. *Agr. Forest Meteorol.* 94, 269-273.

1265 Lhomme, J.P., Monteny, B., 2000. Theoretical relationship between stomatal resistance and
1266 surface temperatures in sparse vegetation. *Agr. Forest Meteorol.* 104, 119-131.

1267 Lhomme, J.P., Vacher, J.J., Rocheteau, A., 2007. Estimating downward long-wave radiation
1268 on the Andean Altiplano. *Agr. Forest Meteorol.* 145, 139-148.

1269 Lhomme, J.P., Montes, C., Jacob, F., Prévot, L., 2012. Evaporation from heterogeneous and
1270 sparse canopies: on the formulations related to multi-source representations. *Bound.-Lay.*
1271 *Meteorol.* 144, 243-262.

1272 Mahfouf, J.-F., and J. Noilhan, 1991. Comparative study of various formulations of
1273 evaporation from bare soil using in-situ data. *J. Appl. Meteorol.*, 30, 1354-1365.

1274 Maxwell, R.M., Miller, N.L., 2005. Development of a coupled land surface and groundwater
1275 model. *J. Hydrometeorol.* 6, 233-247.

1276 Monteith, J.L., 1965. Evaporation and the environment, in: *The state and movement of water*
1277 *in living organisms*, XIX symposium, Soc. Exp. Biol., Swansea, Cambridge University
1278 Press, 205:234.

1279 Morlat, R., Jacquet A., 2003. Grapevine root system and soil characteristics in a vineyard
1280 maintained long-term with or without interrow sward. *Am. J. Enol. Vitic.* 54, 1-7.

1281 Moussa, R., Chahinian, N., Bocquillon, C., 2007. Distributed hydrological modelling of a
1282 Mediterranean mountainous catchment — Model construction and multi-site validation. *J.*
1283 *Hydrol.* 337, 35-51.

1284 Norman, J.M., Kustas, W.P., Humes, K.S., 1995. Source approach for estimating soil and
1285 vegetation energy fluxes in observations of directional radiometric surface temperature.
1286 *Agr. Forest Meteorol.* 77, 263-293.

1287 Ortega-Farias, S., Carrasco, M., Olioso, A., Acevedo, C., Poblete, C., 2007. Latent heat flux
1288 over Cabernet Sauvignon vineyard using the Shuttleworth and Wallace model. *Irrigation*
1289 *Sci.* 25, 161–170.

- 1290 Ortega-Farias, S., Poblete-Echeverría, C., Brisson, N., 2010. Parameterization of a two-layer
1291 model for estimating vineyard evapotranspiration using meteorological measurements.
1292 Agr. Forest Meteorol. 150, 276-286.
- 1293 Padro, J., Massman, W.J., Den Hartog, G., Neumann, H.H., 1994. Dry deposition velocity of
1294 O₃ over a vineyard obtained from models and observations: The 1991 California ozone
1295 deposition experiment. Water Air Soil Pollut. 75, 307-323.
- 1296 Paré, N., 2011. Construction d'un modèle couplé pression-impact pour l'expérimentation
1297 virtuelle de pratiques culturales à l'échelle de petits bassins versants. PhD Thesis,
1298 Montpellier SupAgro. Montpellier, France. 300p.
- 1299 Pellegrino, A., Lebon, E., Simonneau, T.M., Wery, J., 2005. Towards a simple indicator of
1300 water stress in grapevine (*Vitis vinifera* L.) based on the differential sensitivities of
1301 vegetative growth components. Aust. J. Grape Wine Res. 11, 306-315.
- 1302 Pieri, P., 2010a. Modelling radiative balance in a row-crop canopy: Cross-row distribution of
1303 net radiation at the soil surface and energy available to clusters in a vineyard. Ecol. Model.
1304 221, 802-811.
- 1305 Pieri, P., 2010b. Modelling radiative balance in a row-crop canopy: Row-soil surface net
1306 radiation partition. Ecol. Model. 221, 791-801.
- 1307 Pieri, P., Gaudillère, J.P., 2003. Sensitivity to training system parameters and soil surface
1308 albedo of radiation intercepted by vine rows. Vitis. 42, 77-82.
- 1309 Poblete-Echeverria, C., Ortega-Farias, S., 2009. Estimation of actual evapotranspiration for a
1310 drip-irrigated Merlot vineyard using a three-source model. Irrigation Sci. 28, 65-78.
- 1311 Pradel, C., Pieri, P., 2000. Influence of a grass layer on vineyard soil temperature. Aust. J.
1312 Grape Wine Res. 6, 59-67.
- 1313 Raes, D., Deproost, P., 2003. Model to assess water movement from a shallow water table to
1314 the root zone. Agr. Water Manage. 62, 79-91.
- 1315 Rana, G., Katerji, N., 2008. Direct and indirect methods to simulate the actual
1316 evapotranspiration of an irrigated overhead table grape vineyard under Mediterranean
1317 conditions. Hydrol. Process. 22, 181-188.
- 1318 Raupach, M.R., 1989. A practical Lagrangian method for relating scalar concentrations to
1319 source distributions in vegetation canopies. Q. J. Roy. Meteorol. Soc. 115, 609-632.
- 1320 Riou, C., Pieri, P., Valancogne, C., 1987. Variation de la vitesse du vent à l'intérieur et au-
1321 dessus d'une vigne. Agr. Forest Meteorol. 39, 143-154.
- 1322 Riou, C., Valancogne, C., Pieri, P., 1989. Un modèle simple d'interception du rayonnement
1323 solaire par la vigne - Vérification expérimentale. Agronomie. 9, 441-450.

- 1324 Riou, C., Pieri, P., Le Clech, B., 1994. Consommation d'eau de la vigne en conditions
1325 hydriques non limitantes. Formulation simplifiées de la transpiration. *Vitis*. 33, 109-115.
- 1326 Rodriguez-Iturbe, I., 2000. Ecohydrology: A hydrologic perspective of climate-soil-
1327 vegetation dynamics. *Water Resour. Res.* 36, 3-9.
- 1328 Saux-Picart, S., Ottlé, C., Perrier, A., Decharme, B., Coudert, B., Zribi, M., Boulain, N.,
1329 Cappelaere, B., Ramier, D., 2009. SEtHyS_Savannah: A multiple source land surface
1330 model applied to Sahelian landscapes. *Agr. Forest Meteorol.* 149, 1421-1432.
- 1331 Schultz, H.R., 1996. Water relations and photosynthetic response of two grapevine cultivars
1332 of different geographical origin during water stress. *Acta Hortic.* 427, 251-266.
- 1333 Sene, K.J., 1994. Parameterisations for energy transfers from a sparse vine crop. *Agr. Forest*
1334 *Meteorol.* 71, 1-18.
- 1335 Sene, K.J., 1996. Meteorological estimates for the water balance of a sparse vine crop
1336 growing in semiarid conditions. *J. Hydrol.* 179, 259-280.
- 1337 Sellers, P.J., Heiser, M.D., Hall, F.G., 1992. Relations between surface conductance and
1338 spectral vegetation indices at intermediate (100 m² to 15 km²) length scales. *J. Geophys.*
1339 *Res.* 97, 19033–19059.
- 1340 Shuttleworth, W.J., Wallace, J.S., 1985. Evaporation from sparse crops - an energy
1341 combination theory. *Q. J. Roy. Meteor. Soc.* 111, 839-855.
- 1342 Shuttleworth, W.J., Gurney, R.J., 1990. The theoretical relationship between foliage
1343 temperature and canopy resistance in sparse crops. *Q. J. Roy. Meteor. Soc.* 111, 839-855.
- 1344 Sini, F., Boni, G., Caparrini, F., Entekhabi, D., 2008. Estimation of large-scale evaporation
1345 fields based on assimilation of remotely sensed land temperature . *Water. Resour. Res.* 44,
1346 W06410, doi:10.1029/2006WR005574 .
- 1347 Siqueira, M., Katul, G., Porporato, A., 2008. Onset of water stress, hysteresis in plant
1348 conductance, and hydraulic lift: Scaling soil water dynamics from millimeters to meters.
1349 44, W01432, doi:10.1029/2007WR006094.
- 1350 Soylu, M.E., Istanbuluoglu, E., Lenters, J.D., Wang, T., 2011. Quantifying the impact of
1351 groundwater depth on evapotranspiration in a semi-arid grassland region. *Hydrol. Earth*
1352 *Syst. Sci.* 15, 787-806.
- 1353 Spano, D., Snyder, R.L., Sirca, C., Duce, P., 2009. ECOWAT – A model for ecosystem
1354 evapotranspiration estimation. *Agr. Forest Meteorol.* 149, 1584-1596.
- 1355 Stewart, J.B., 1988. Modelling surface conductance of pine forest. *Agr. Forest. Meteorol.* 43,
1356 19-35.
- 1357 Taconet, O., Bernard, R., Vidal-Madjar, D., 1986. Evapotranspiration over an agricultural

- 1358 region using a surface flux/temperature model based on NOAA-AVHRR data. *J. Clim.*
1359 *Appl. Meteorol.* 25, 284-307.
- 1360 Trambouze, W., Bertuzzi, P., Voltz, M., 1998. Comparison of methods for estimating actual
1361 evapotranspiration in a row-cropped vineyard. *Agr. Forest Meteorol.* 91, 193-208.
- 1362 Trambouze, W., Voltz, M., 2001. Measurement and modelling of the transpiration of a
1363 Mediterranean vineyard. *Agr. Forest Meteorol.* 107, 153-166.
- 1364 Tuzet, A., Perrier, A., Leuning, R., 2003. A coupled model of stomatal conductance,
1365 photosynthesis and transpiration. *Plant Cell Environ.* 26, 1097-1116.
- 1366 Van den Hurk, B.J.J.M., McNaughton, K.G., 1995. Implementation of near-field dispersion in
1367 a simple two-layer surface resistance model. *J. Hydrol.* 166, 293-311.
- 1368 Vaudour, E., 2003. *Les terroirs viticoles*. Dunod, Paris, 312p.
- 1369 Verhoef, A., Allen, S.J., 2000. A SVAT scheme describing energy and CO₂ fluxes for multi-
1370 component vegetation: calibration and test for a Sahelian savannah. *Ecol. Model.* 127,
1371 245-267.
- 1372 Vervoort, R.W., van der Zee, S.E.A.T.M., 2008. Simulating the effect of capillary flux on the
1373 soil water balance in a stochastic ecohydrological framework. *Water Resour. Res.* 44,
1374 W08425, doi:10.1029/2008WR006889.
- 1375 Volpe, V., Marani, M., Albertson, J.D., Katul, G., 2013. Root controls on water redistribution
1376 and carbon uptake in the soil-plant system under current and future climate. *Adv. Water*
1377 *Resour.* 60, 110-120.
- 1378 Weiss, A., Allen, L.H.J., 1976. Air flow patterns in vineyard rows. *Agric. Meteorol.* 16, 329-
1379 342.
- 1380 Winkel, T., Rambal, S., 1990. Stomatal conductance of some grapevines growing in the field
1381 under Mediterranean environment. *Agr. Forest Meteorol.* 51, 107-121.
- 1382 Winkler, A.J., Williams, W.O., 1939. The heat required to bring Tokay grapes to maturity.
1383 *Proceedings of the American Society of Horticultural Science.* 37, 650-652.
- 1384 Wu, A., Black, A., Verseghy, D.L., Bailey, W.G., 2001. Comparison of two-layer and single-
1385 layer canopy models with Lagrangian and *K*-theory approaches in modeling evaporation
1386 from forests. *Int. J. Climatol.* 21, 1821-1839.
- 1387 Yi, C. 2008. Momentum transfer within canopies, *J. Appl. Meteorol. Climatol.* 47, 262-275.
- 1388 Zhang, B.Z., Kang, S.Z., Li, F.S., Zhang, L., 2008. Comparison of three evapotranspiration
1389 models to Bowen ratio-energy balance method for a vineyard in a desert region of
1390 northwest China. *Agr. Forest Meteorol.* 148, 1629-1640.
- 1391 Zhang, Y.-K., Schilling, K.E., 2006. Effects of land cover on water table, soil moisture

1392 evapotranspiration, and groundwater recharge: A field observation and analysis. J.
1393 Hydrol. 319, 328-338.

1394 Zhang, B., Kang, S., Zhang, L., Tong, L., Du, T., 2009. An evapotranspiration model for
1395 sparsely vegetated canopies under partial root-zone irrigation. Agr. Forest Meteorol. 149,
1396 2007-2011.

1397 **Table 1.** Uncertainty range and final values for the fitted parameters of the plant-atmosphere model, as obtained from the MCIP calibration.

1398

Parameter	Equation	Description (units)	Initial uncertainty range	Final calibrated value
Biophysical parameters				
c	7 and 15	Extinction coefficient of main foliage (-)	0.3 – 0.7	0.45
β_{vs}	9	Soil heat flux fraction for vegetated soil (-)	0.1 – 0.4	0.28
β_{bs}	10	Soil heat flux fraction for bare soil (-)	0.2 – 0.5	0.38
$g_{x,f}$	17	Maximal stomatal conductance (main foliage) (m s^{-1})	$1.25 \times 10^{-3} - 1.2 \times 10^{-2}$	3.3×10^{-3}
$g_{x,vs}$	17	Maximal stomatal conductance (vegetated soil) (m s^{-1})	$3.3 \times 10^{-3} - 1.0 \times 10^{-2}$	3.7×10^{-3}
a_f	16	Foliage albedo (-)	0.1 – 0.4	0.24
a_{bs}	16	Bare soil albedo (-)	0.2 – 0.5	0.3
a_{vs}	16	Grass albedo (-)	0.15 – 0.35	0.25
Empirical parameters				
K_1^f	18	Parameter of PAR stress function (main foliage) ($\mu\text{mol m}^{-2} \text{s}^{-1}$)	80 – 200	150
K_1^{vs}	18	Parameter of PAR stress function (vegetated soil) (W m^{-2})	80 – 140	112
K_2^f	19	Parameter of D_a stress function (main foliage) (kPa^{-1})	$1.575 \times 10^{-4} - 3.125 \times 10^{-4}$	2.0×10^{-4}
K_2^{vs}	19	Parameter of D_a stress function (vegetated soil) (kPa^{-1})	$3.5 \times 10^{-2} - 1.05 \times 10^{-1}$	7.0×10^{-2}
K_3^f	20	Parameter of θ stress function (main foliage) (-)	10 – 100	35
K_3^{vs}	20	Parameter of θ stress function (vegetated soil) (-)	10 – 100	45
A_1	21	Parameter of bare soil resistance (-)	5 – 15	8
B_1	21	Parameter of bare soil resistance (-)	1 – 10	5

1399

1400 **Table 2.** Measured and estimated values of parameters used in the soil water balance model.

1401

Soil parameter	Value	Units	Informative source
Soil profile description			
$\theta_{n,1}$	0.05	$\text{m}^3 \text{m}^{-3}$	Trambouze and Voltz, 2001
$\theta_{n,2} = \theta_{n,3} = \theta_{f,wp}$	0.15	$\text{m}^3 \text{m}^{-3}$	Trambouze and Voltz, 2001
$\theta_{fc,1}$	0.246	$\text{m}^3 \text{m}^{-3}$	<i>Measured</i>
$\theta_{fc,2}$	0.268	$\text{m}^3 \text{m}^{-3}$	<i>Measured</i>
$\theta_{fc,3}$	0.331	$\text{m}^3 \text{m}^{-3}$	<i>Measured</i>
p_1	0.16	Fraction	<i>Measured</i>
p_2	0.20	Fraction	<i>Measured</i>
p_3	0.16	Fraction	<i>Measured</i>
Capillary rise equations			
$\Psi_{s,3}$	0.63	m	Clapp and Hornberger (1978)
Ψ_G	0.63	m	Clapp and Hornberger (1978)
$\theta_{s,3}$	0.476	$\text{m}^3 \text{m}^{-3}$	Clapp and Hornberger (1978)
$K_{s,3}$	2.45×10^{-6}	m s^{-1}	Clapp and Hornberger (1978)
b_3	8.52	-	Clapp and Hornberger (1978)
Reservoirs depth			
z_1	0.05	m	<i>Locally estimated</i>
z_2	0.50	m	<i>Locally estimated</i>
z_R	2.0	m	<i>Locally estimated</i>

1402

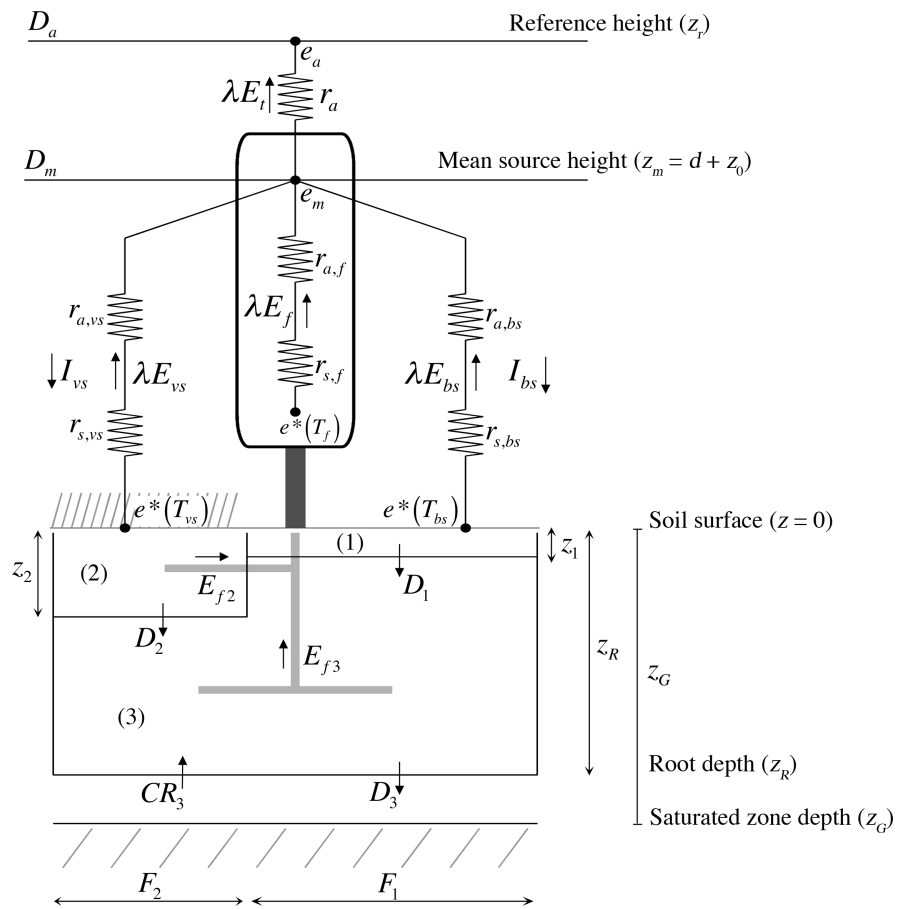
1403

1404

1405 **Fig. 1.** Schematic representation of the three-source evaporation model and the soil water
 1406 transfer model. $r_{a,f}$ is the bulk boundary-layer resistance of the main foliage for water vapor
 1407 transfer ($r_{a,f} = 2r_{a,f,h}$). See list of symbols for other parameters definition. Numbers (1), (2) and
 1408 (3) denote the three soil reservoirs related to evaporation components f (main foliage), vs
 1409 (vegetated soil) and bs (bare soil).

1410

1411



1412

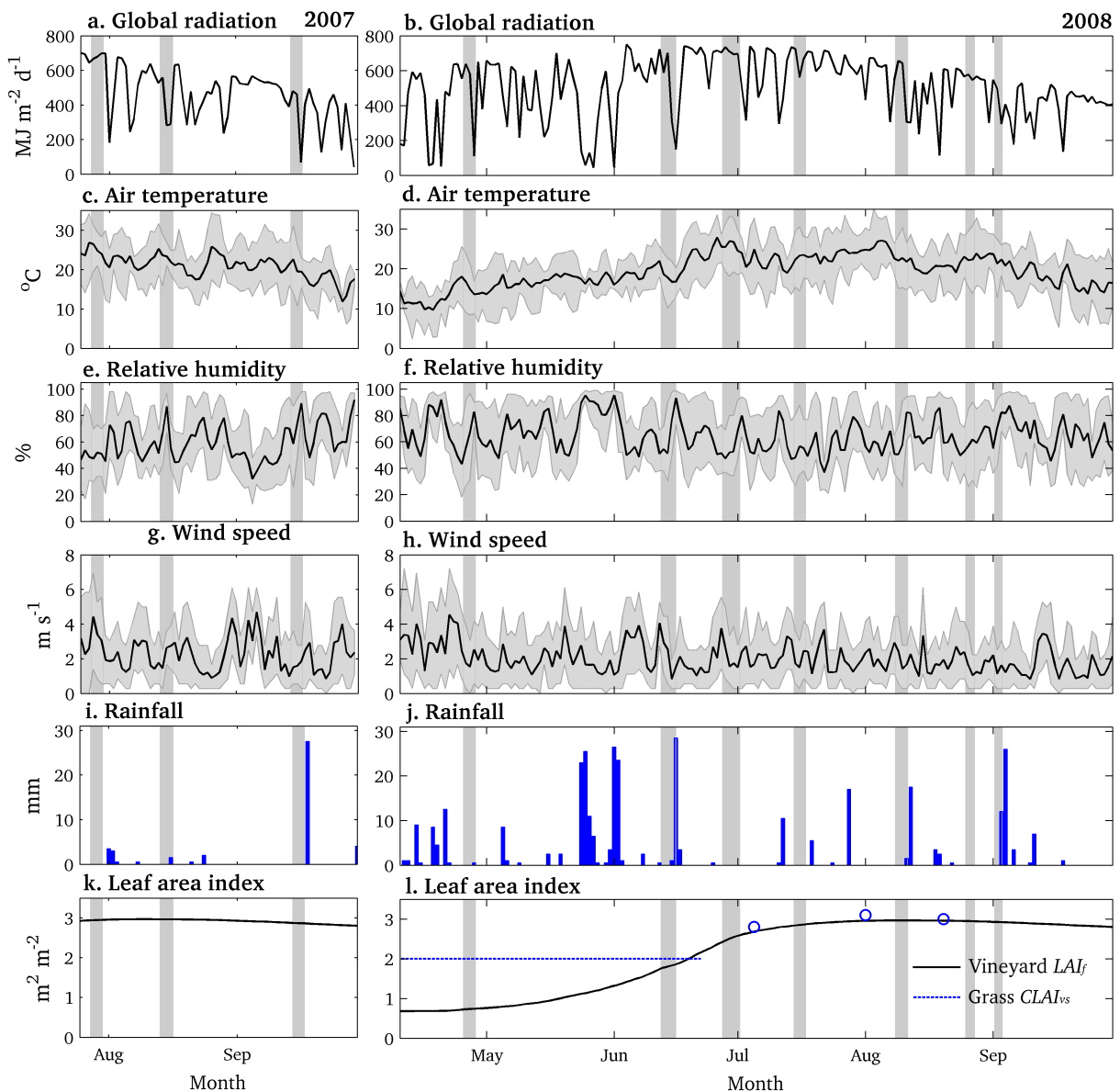
1413

1414

1415

1416 **Fig. 2.** Time series of meteorological variables, as measured during the simulation period, and
1417 used for model forcing. Gray shaded bars show periods of evaporation measurements used for
1418 model validation. (a)-(b) Daily incident solar radiation; (c)-(d) daily mean air temperature;
1419 (e)-(f) daily mean relative humidity; (g)-(h) daily mean wind speed; (i)-(j) daily accumulated
1420 precipitation. Also, simulated LAI_f (Eq. (37)) and estimated $CLAI_{vs}$ are shown in (k)-(l).
1421 Circles in (l) are LAI_f measurements. Shaded intervals in (c) to (h) represent daily minimum
1422 and maximum values. Abscise labels denote the beginning of each month.

1423



1424

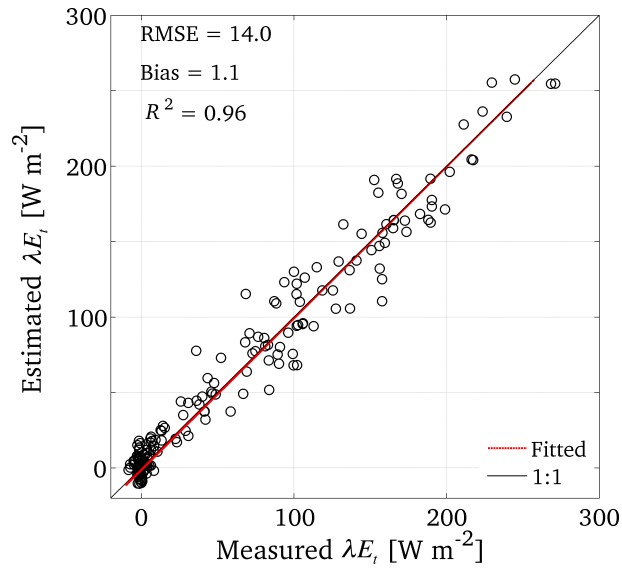
1425

1426 **Fig. 3.** Scatter plot of hourly measured and simulated total latent heat flux (λE_t).

1427

1428

1429



1430

1431

1432

1433

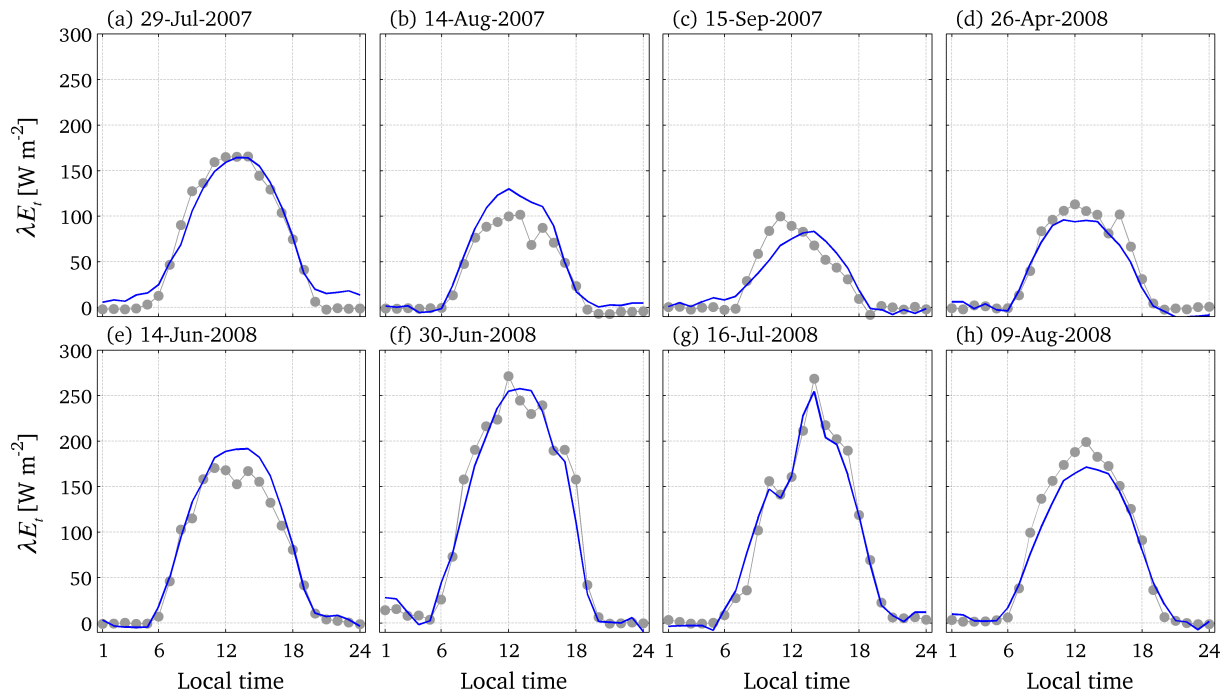
1434

1435

1436 **Fig. 4.** Time series of simulated (lines) and measured (circles) hourly latent heat flux (λE_t) for
1437 eight observation days.

1438

1439



1440

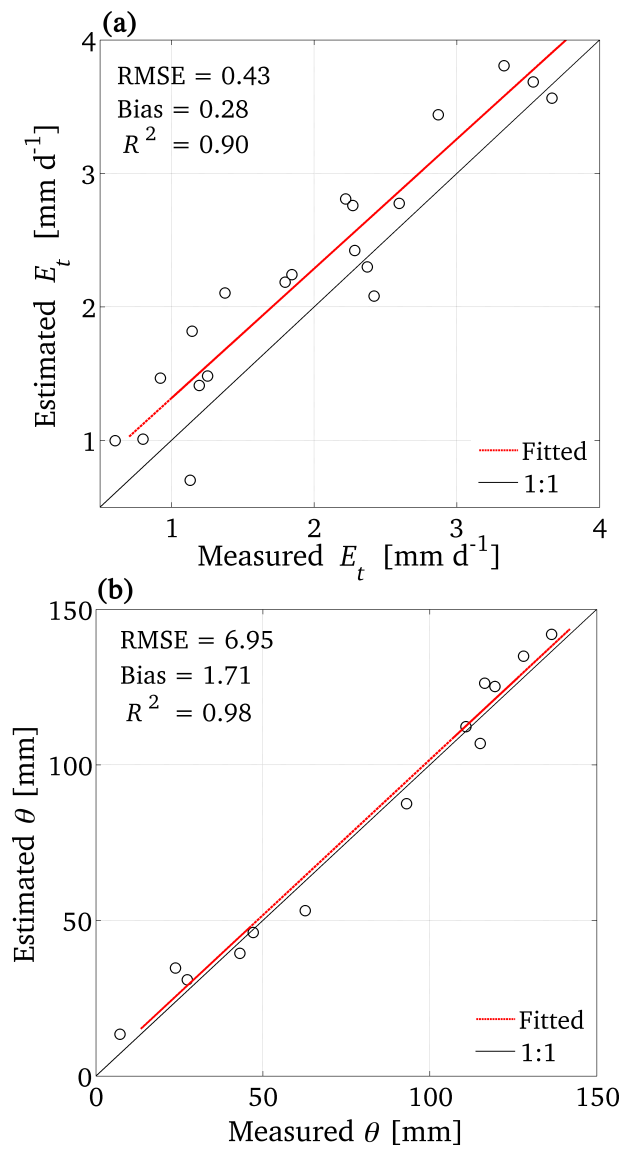
1441

1442

1443 **Fig. 5.** Scatter plot of daily (a) total evaporation (E_t) and (b) soil water content (θ) as
1444 measured and as simulated by the model. In (a) only days with 24 hours of measurements
1445 were included.

1446

1447



1448

1449

1450

1451

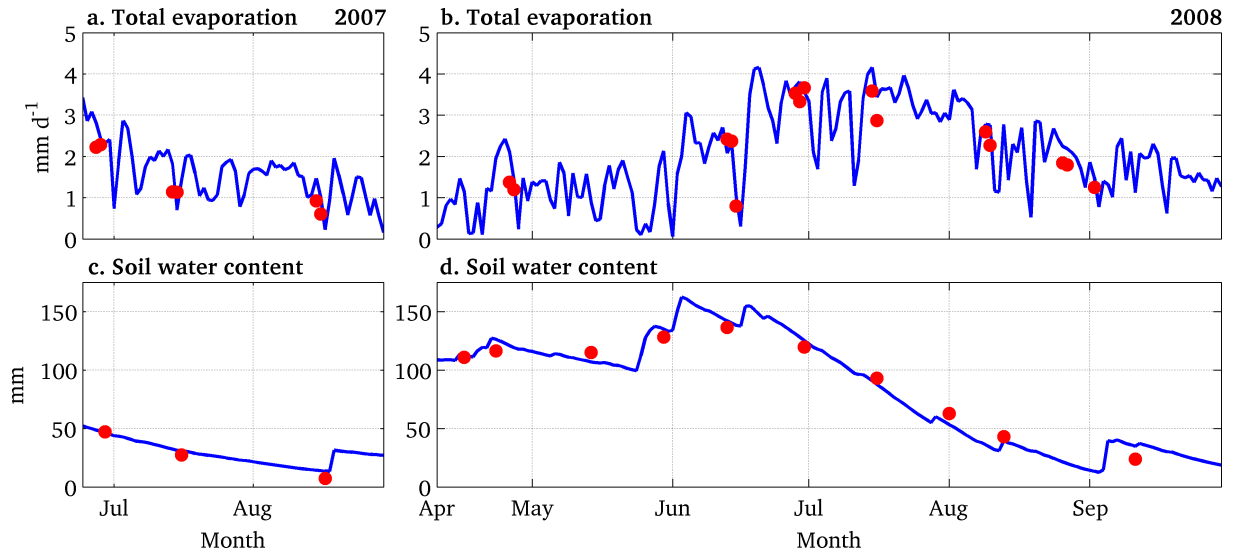
1452

1453

1454

1455 **Fig. 6.** Time series of (a) simulated (line) and observed (circles) daily total evaporation, and
1456 (b) simulated (line) and observed (circles) integrated profile volumetric soil water content.
1457 Abscissa labels denote the beginning of each month.

1458



1459

1460

1461

1462

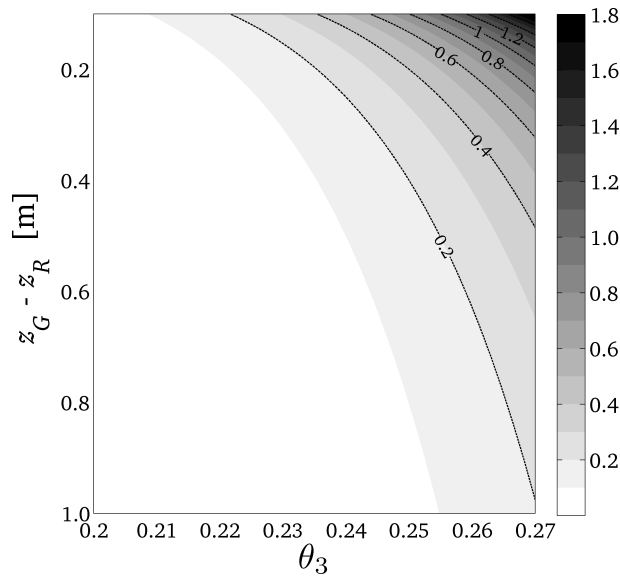
1463

1464

1465 **Fig. 7.** Capillary flow (contours in mm d^{-1}) between saturated zone and reservoir (3) as a
1466 function of the distance between water table (z_G) and root zone depth (z_R) and soil water
1467 content of reservoir (3). Upward flow is taken as positive values.

1468

1469



1470

1471

1472

1473

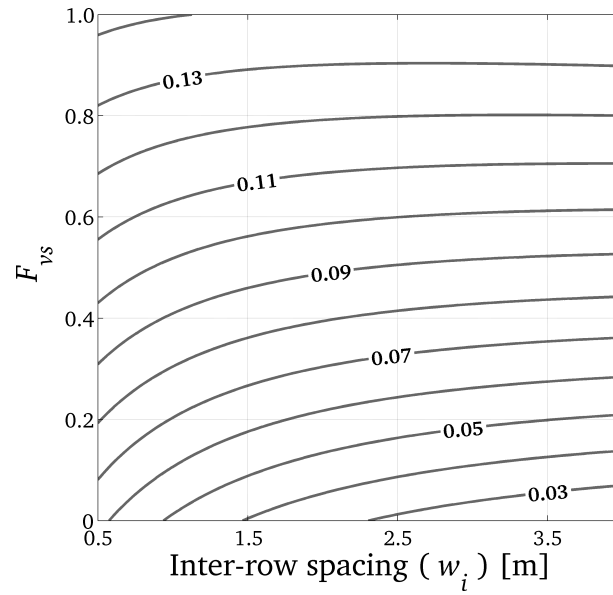
1474

1475

1476 **Fig. 8.** Simulated total evaporation (contours in mm h^{-1}) as a function of the spacing between
1477 vine rows w_i and the grass cover fraction F_{vs} .

1478

1479



1480

1481